12-2014

Applications of magnetostrictive materials in the real-time monitoring of vehicle suspension components

Raul Estrada
University of Texas-Pan American

APPLICATIONS OF MAGNETOSTRICTIVE MATERIALS IN THE REAL-TIME MONITORING OF VEHICLE SUSPENSION COMPONENTS

A Thesis

by

RAUL ESTRADA

Submitted to the Graduate School of
The University of Texas-Pan American
In partial fulfillment of the requirements for the degree of

MASTER OF SCIENCE

December 2014

Major Subject: Electrical Engineering

APPLICATIONS OF MAGNETOSTRICTIVE MATERIALS IN THE REAL-TIME MONITORING OF VEHICLE SUSPENSION COMPONENTS

A Thesis
by
RAUL ESTRADA

COMMITTEE MEMBERS

Dr. Constantine Tarawneh
Co-Chair of Committee

Dr. Heinrich Foltz
Co-Chair of Committee

Dr. Junfei Li
Committee Member

December 2014

ABSTRACT

Estrada, Raul, Applications of Magnetostrictive Materials in the Real-Time Monitoring of Vehicle Suspension Components. Master of Science (MS), December, 2014, 100 pp., 6 tables, 81 figures, 9 references.

The purpose of this project is to explore applications of magnetostrictive materials for real-time monitoring of railroad suspension components, in particular bearings. Monitoring of such components typically requires the tracking of temperature vibration and load. In addition, real-time, long-term monitoring can be greatly facilitated through the use of wireless, self-powered sensors. Magnetostrictive materials, such as Terfenol-D, have the potential to address both requirements. Currently, piezoelectrics are used for many load and energy harvesting applications; however, they are fragile and are difficult to use for static load measurements. Magnetostrictive metals are tougher, and their property of variable permeability when stressed can be utilized to measure static loads. A prototype load sensor was successfully fabricated and characterized yielding less than 10% error under normal operating conditions. Energy harvesting experiments generated a little over 80 mW of power, which is sufficient to run low-power condition monitoring systems.

DEDICATION

The constant support and encouragement of my family and friends was the primary driving factor that led to the completion of my thesis. My dad, Javier Estrada, and my brother, Christian Estrada both inspired and motivated me through example. My mother, Carmen Estrada, and my sister, Wendy Estrada provided much of the emotional support that kept me going. My friends, Victor Gutierrez, Jay Pedrogosa, and Richard Garza always encouraged me while helping me keep a healthy level of sanity throughout the process. Thank you all for everything, you mean the world to me.

ACKNOWLEDGMENTS

Before all else, I want to take this opportunity to thank James Bantz, without whom I would not have challenged myself and taken on research. His support and advice led me to aspire for more than the bare minimum.

That being said, Dr. Tarawneh gave me the opportunity to work as part of his research group, providing not only guidance and mentoring, but also giving me real world applications for the skills I learned during my studies. Through his leadership, I was able to coauthor one paper and be the primary author in another. I am truly grateful to have worked on such an auspicious research group.

Dr. Foltz was always available for questions and advice regarding the project. It is thanks to his support that the project came as far as it did. His knowledge and willingness to help allowed me to continue working without worry of being in over my head.

Thanks to Rene Moreno for all the effort making much of the work possible. Without your machining expertise and willingness to do what needed to be done, the project would have taken much longer to complete. From testing to machining to modeling, your input was always appreciated.

Tom, Amy, Dan, Rigo, Allen, Carlos, and Ricardo, while I didn't often call on you for help, it means a lot that you were always willing to offer it.

TABLE OF CONTENTS

LIST OF TABLES

LIST OF FIGURES

CHAPTER I.

BACKGROUND

The first man-hauled railways are credited to Periander, one of the Seven Sages of Greece in the 6th century. It was through his invention that national markets became viable and allowed for a lower cost for goods. In the 18th century, the British developed the steam engine which allowed for the construction of mainline railways. It was not until the mid 19th century that diesel-electric engines began replacing steam powered locomotives. As a result of the increasing demand for railway transportation, regulations were put in place to ensure that every measure is taken to reduce the possibility of derailments. There are various standards to which a railcar must adhere to in order to be deemed safe for operation. In addition to these standards, the Association of American Railroads (AAR) has created and enforced several wayside detection policies for the removal of bearings suspected of abnormal operation. The University of Texas-Pan American (UTPA) Railroad Research Group has been conducting several studies in order to help expedite innovations in bearing health monitoring systems. During the last six years, the UTPA Railroad Research Group has been working with on-board health monitoring systems that were created to replace the current wayside detection systems. A number of bearing health indicators are analyzed by these systems, such as: applied load, vibration signals, and temperature histories. It is the aim of this research group to prove the viability of these systems, thereby leading to an improved bearing health monitoring system.

1.1 Wayside Detection

The railroad industry foresaw a need for bearing health monitoring to reduce the risk of derailment. To this end, infrared temperature detectors were implemented in the early 1960s in order to try and identify distressed bearings. These sensors, commonly referred to as hot box detectors

are placed at intervals of 15 to 40 miles, depending on the location of the track. A common setup is illustrated in Figure 1.1. These sensors take the instantaneous temperature of bearings as they roll past them. As a result, they can only identify distressed bearings immediately before or after a failure. In an effort to extend that window of detection, Union Pacific employed a new algorithm capable of detecting distressed bearings that are still below the thresholds set in place by the Association of American Railroads. This algorithm was put into practice in 2002, thus, reducing the number of bearing failures over the past decade. However, this method has resulted in many non-verified bearings. A non verified bearing is one that is flagged as defective, yet upon removal, and inspection is proven to be healthy. Non verified bearings are costly for the railroads, car owners, and customers as they result in unnecessary train stoppages and delays. A staggering 40% of the bearings removed were from 2001 to 2007 were non verified [2].

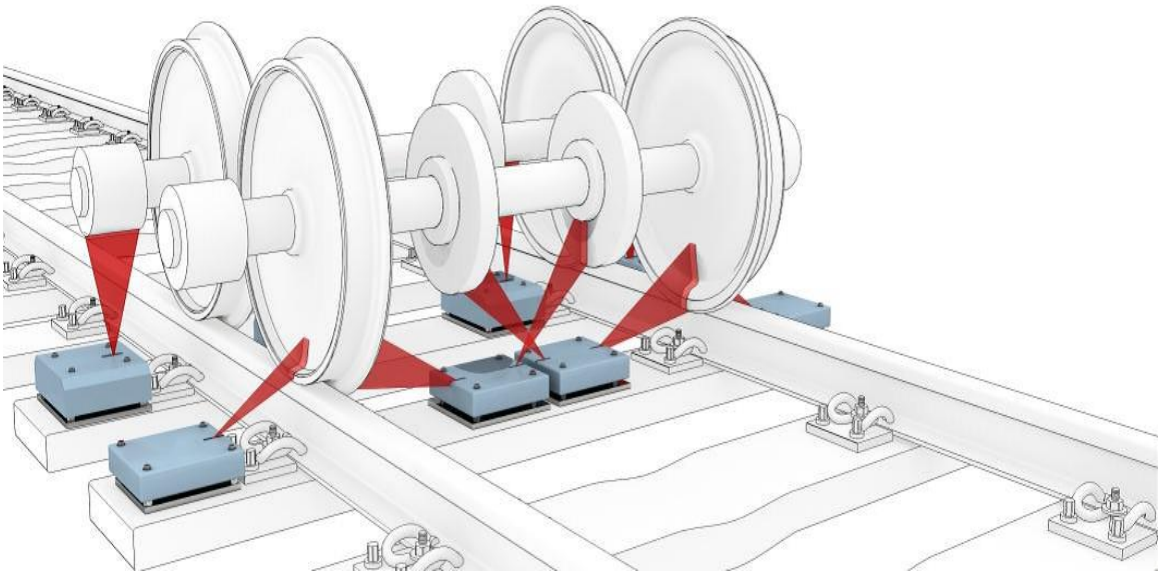

Figure 1.1: Hot Box Detector Setup [2]

1.2 Onboard Monitoring Technology

To combat the issues associated with wayside detection, onboard real-time monitoring of railcar bearings is being developed. These onboard monitoring devices are comprised of three independent sensors that are used to measure: temperature, load, and vibration. Central Monitoring Units

(CMU) are used to collect the readings from numerous sensors, including those used in defect detection. The CMU, presented in Figure 1.2, then communicates through cellular networks and all the information is uploaded to client side servers. After which the data is downloaded from those servers and processed using complex algorithms that can identify defective bearings just as they are beginning to spall. This gives the railcar owner ample time to inspect and swap out the defective bearing at their earliest convenience, i.e. when the train is stopped in a rail yard.

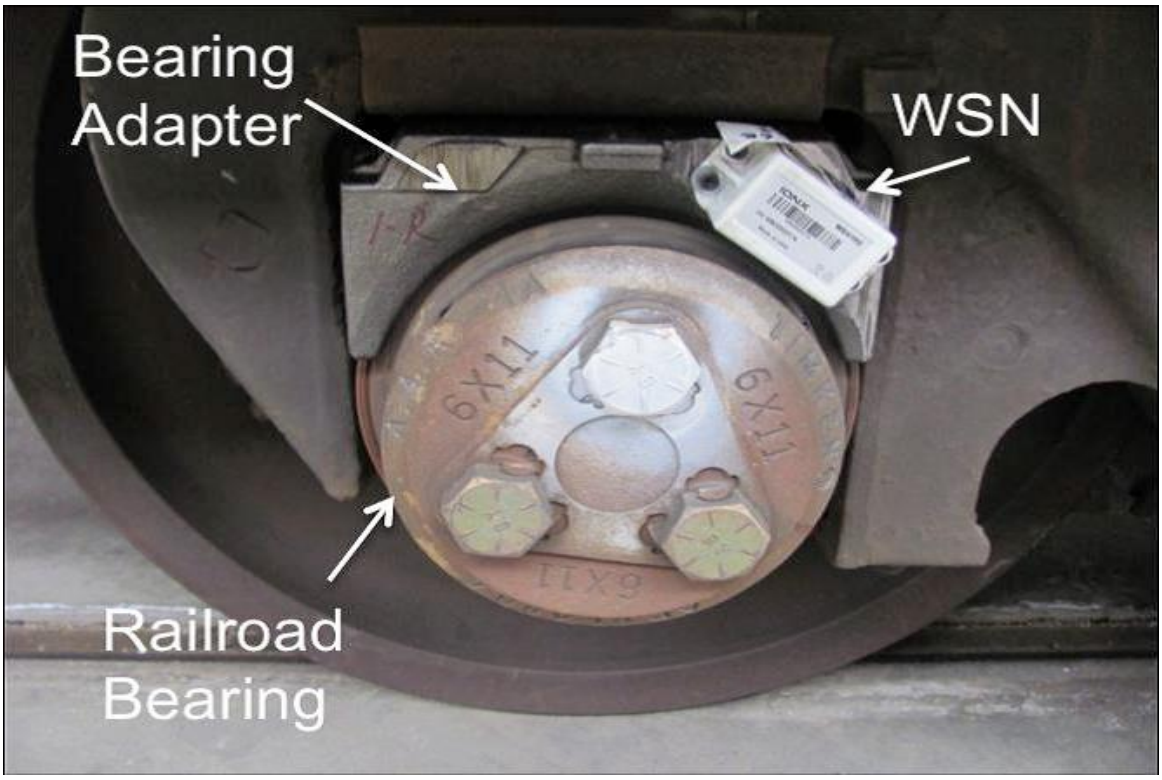

Figure 1.2: WSN Placement [2]

1.3 Motivation

In practice, implementation of real-time, onboard bearing health monitoring, requires compromise between cost efficiency and performance. The method for properly identifying bearings is frequently under revision. The goals of this project are to design a load sensor using Terfenol-D and to generate enough power so that things like sampling rate and reporting frequency can be improved rather than sacrificed. Currently, piezoelectrics are used for load detection and accelerometers for

vibration detection. However, piezoelectrics are ceramic in nature and very brittle, making them unfavorable for the railway applications. Magnetostrictive alloys such as Terfenol-D are much more durable and impact resistant, thereby more suited to the application of bearing health monitoring. Through the use of the Villari effect (the inverse of the magnetostrictive effect), it is possible to transform a change in the applied force into a change in inductance. This same type of excitation can be used to generate power. If the electromagnetic problems posed in this project can be accounted for, the creation and characterization of this single device will be able to replace two important components in on-board monitoring equipment: the load sensor and the battery.

1.4 Background & Applications of Terfenol-D

Terfenol-D ($Tb_xDy_{1-x}Fe_2(x \sim 0.3)$) is a material which has the highest magnetostriction of any alloy. Developed in 1970, it is named after the metals it contains and the laboratory in which it was discovered: Terbium (Ter), Iron (fe), Naval Ordnance Laboratory (nol), Dysprosium (D) [1]. The original intended application of the material was in naval sonar systems, using a magnetic field generated through electromagnetism to cause it to expand and contract, thus generating ultrasonic waves necessary for sonar. It was later discovered to have many other useful applications, such as: actuators, acoustic and ultrasonic transducers, and magneto-mechanical sensors. All of these applications apply the magnetostrictive properties of Terfenol-D, that is, the effect some alloys have to change dimensions under an applied magnetic field. Throughout this project, the inverse effect will be explored, i.e. the Villari effect. The Villari effect, also known as the magnetoelasticity, is the name given to the change of relative magnetic permeability of material when mechanical stress is applied. The most common application of the magnetoelastic effect is in the development of force sensors.

1.5 Literature Review

1.5.1 Magnetoelastic Force Sensors

Much work has been done to investigate the applications of magnetoelastic materials. One such application is the creation of force sensors based on magnetostrictive materials. In this configuration, a robust and simple single coil is wound around a Terfenol-D core and the inductance is measured across various stages of stress. An example of this configuration is provided in Figure 1.3. During this particular study, the Terfenol-D core was excited with a relatively small excitation voltage ($0-4.5V$) and compressed over a range of $0-2000N$, the relative magnetic resistance change is then measured. The results of this study can be seen in Figure 1.4. [3]

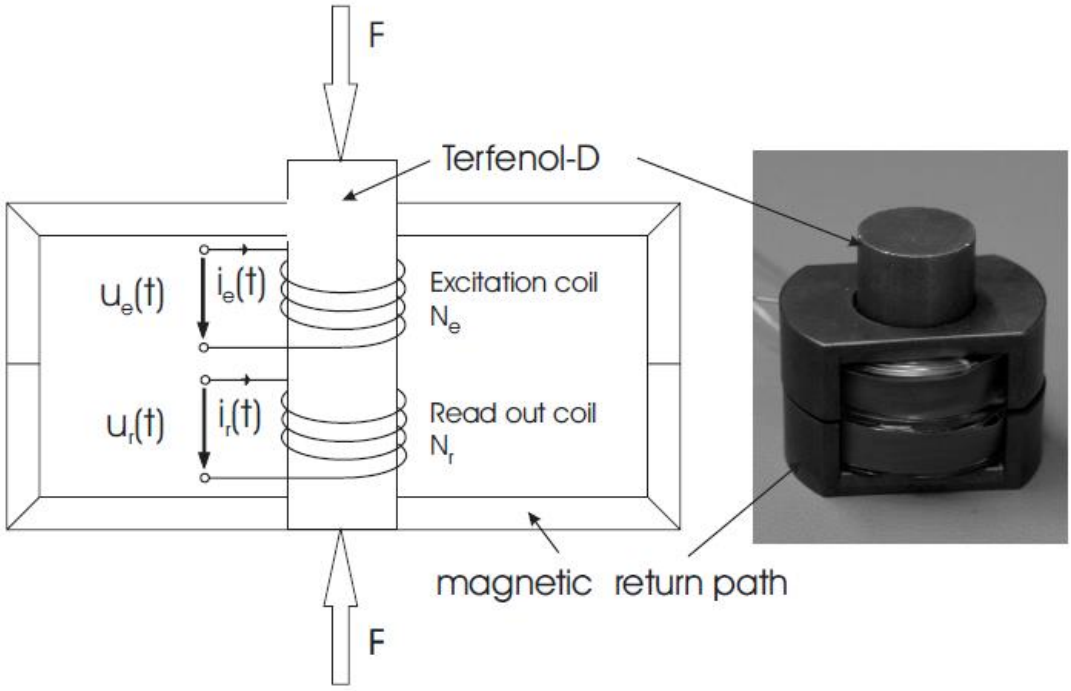

Figure 1.3: Magnetoelastic Force Sensor [3]

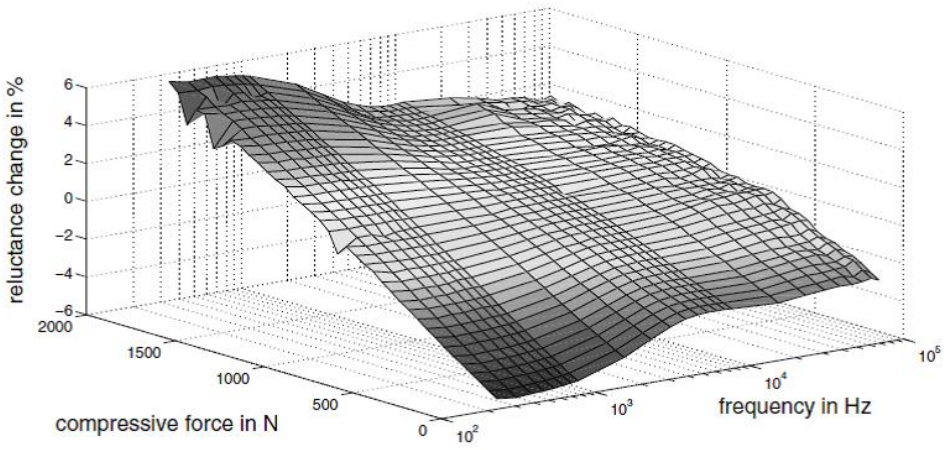

Figure 1.4: Reluctance Change Response

1.5.2 Energy Generation

Magnetoelectric energy generation is a new and exciting technology in terms of wireless sensor networks. Multiple devices that utilize this concept have been created and characterized. Some use piezoelectric components in conjunction with mechanical anchors to harvest vibrational energy as shown in Figure 1.5. The ultrasonic horn enhances the energy density from the larger end, transferring it to the narrower end. Such a device has been proven to generate as much as $20\mu W$ of power. [4]

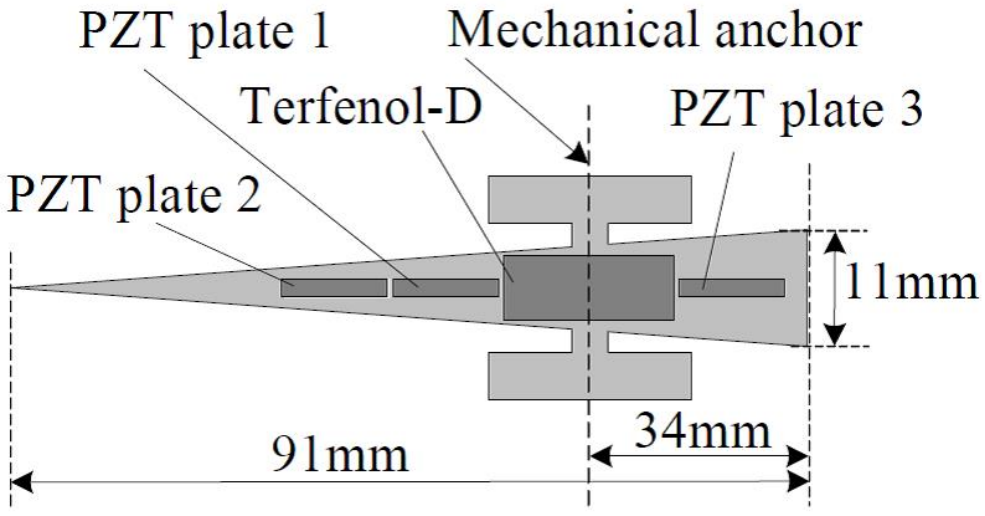

Figure 1.5: Vibration Energy Harvesting Mechanism [4]

Other systems use a cantilever beam paired with a magnetic circuit to harvest the energy from a magnetoelectric transducer consisting of a Terfenol-D/PMN-PT/Terfenol-D laminate. Standard neodymium magnets are used to create a particular field. The arrangement of these components is shown in Figure 1.6. When the harvester is excited, the magnetic field generated by the magnets moves. This change in magnetic field causes the Terfenol-D laminate to expand and contract. That change in shape causes the piezoelectric plates to stress, thereby generating electricity. This configuration has been proven to yield almost $2mW$ of power. [5]

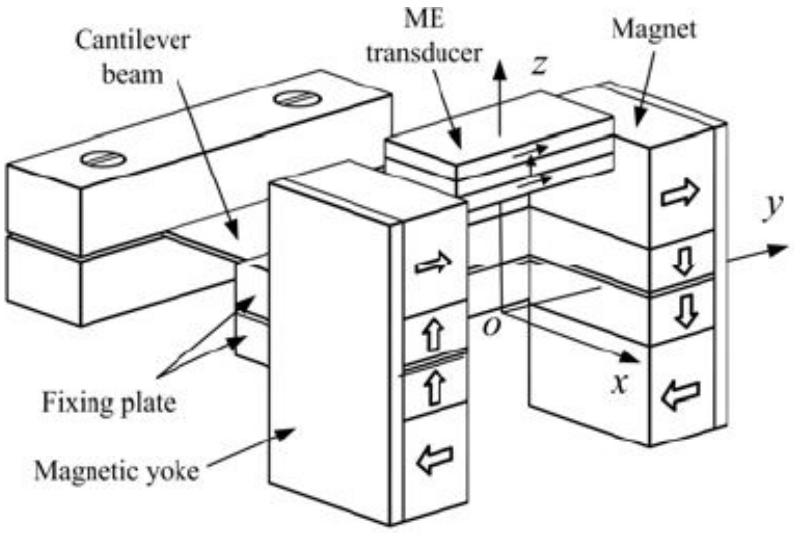

Figure 1.6: Vibration Energy Harvesting System [5]

All of these systems use Terfenol-D in its magnetostrictive capacity to stress a piezoelectric layer, generating high voltage, yet low power. It is the goal of this project to use a bigger sample of Terfenol-D in a magnetoelastic configuration to create a considerably larger amount of power, even if it is at a lower voltage. Rather than harvesting vibrational energy, the compression associated with that vibration will be utilized.

CHAPTER II.

MATERIAL CHARACTERIZATION AND INSTRUMENTATION

The Terfenol-D samples initially available for testing are cylindrical pieces of stock measuring 1.3 cm (.512 in) in diameter and 1.27 cm (.500 in) in length. Before conducting any tests on the magnetostrictive properties of the material, it is necessary to establish boundary conditions under which these tests may be performed. A practical approach to finding these thresholds is to measure and verify applicable material properties. The pertinent mechanical properties for the applications under which this sensor would be utilized are: hardness, relative permeability at no load, Young's Modulus, and compressive strength. Each of the properties is measured and verified through various methods: the hardness is obtained using a micro hardness tester, the permeability is calculated through simulation, and the compressive strength is verified with the Material Test System (MTS). These values are then compared to those given by the manufacturer. The physical properties as provided by the manufacturer data sheet are shown in Table 2.1.

Table 2.1: Terfenol-D Physical Properties [1]

TERFENOL-D PHYSICAL PROPERTIES	
Nominal Composition	$Tb_{0.3}Dy_{0.7}Fe_{1.92}$
Mechanical Properties	
Young's Modulus	$25 - 35\ GPA$
Sound Speed	$1640 - 1940\ m/s$
Tensile Strength	$28\ Mpa$
Compressive Strength	$700\ Mpa$
Thermal Properties	
Coefficient of Thermal Expansion	$12\ ppm/°C$
Specific Heat	$0.35\ kJ/kg \cdot K$
Thermal Conductivity	$13.5\ W/m \cdot K$
Electrical Properties	
Resistivity	$58x10 - 8\ O \cdot m$
Curie Temperature	$380°C$
Magnetostrictive Properties	
Strain (estimated linear)	$800 - 100\ ppm$
Energy Density	$14 - 25\ kJ/m^3$
Magnetomechanical Properties	
Relative Permeability	$3 - 10$
Coupling Factor	0.75

2.1 Hardness

From the hardness of the alloy, the behavior of the Terfenol-D core in its operational environment can be characterized, e.g. whether or not it will chip and crack when compressed with a given force. This value is determined using a micro hardness test in accordance with ASTM E92 [9]. The test has a chance of damaging the Terfenol-D core, for this reason, a piece from a previously damaged sample was used. The piece must be set in a polymer puck to ensure stability, as pictured in Figure 2.1. Before proceeding with the test, the surface on which the test will be conducted is inspected for uniformity. This particular sample proved to be very porous and uneven on the surface, as shown in Figure 2.2. Preparing the sample for hardness testing requires: grinding, polishing, and mirroring. The result of these processes is shown in Figure 2.3. Hardness is determined by pressing a small diamond tip onto the surface of the material with a known force and measuring the resulting indention. This process is known as a Vickers hardness test, as is reflected in the units of the resulting measurements (Vickers). The indentation created in the Terfenol-D sample can be seen in Figure 2.4. The Hardness Value (HV) is determined by finding the ratio between Force (F) and Area (A): $HV = F/A$. The area of the indention is defined as: $A = \frac{d^2}{2*sin(136^o/2)}$. These values are listed in Table 2.2. The first section of the table shows the experiments conducted to find the appropriate force to be applied to the material. The ideal force for an accurate hardness test is the largest force that will not cause the sample to fracture.

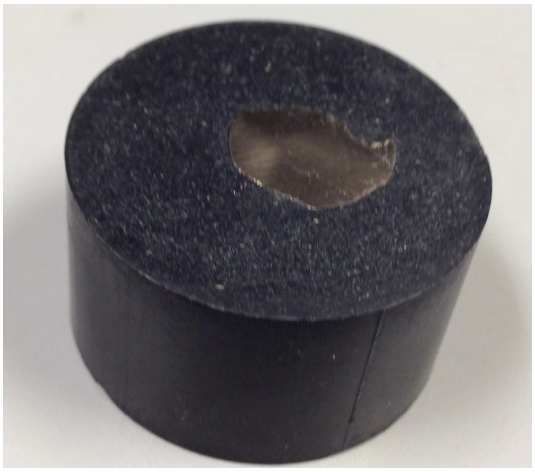

Figure 2.1: Terfenol Set in Polymer Puck

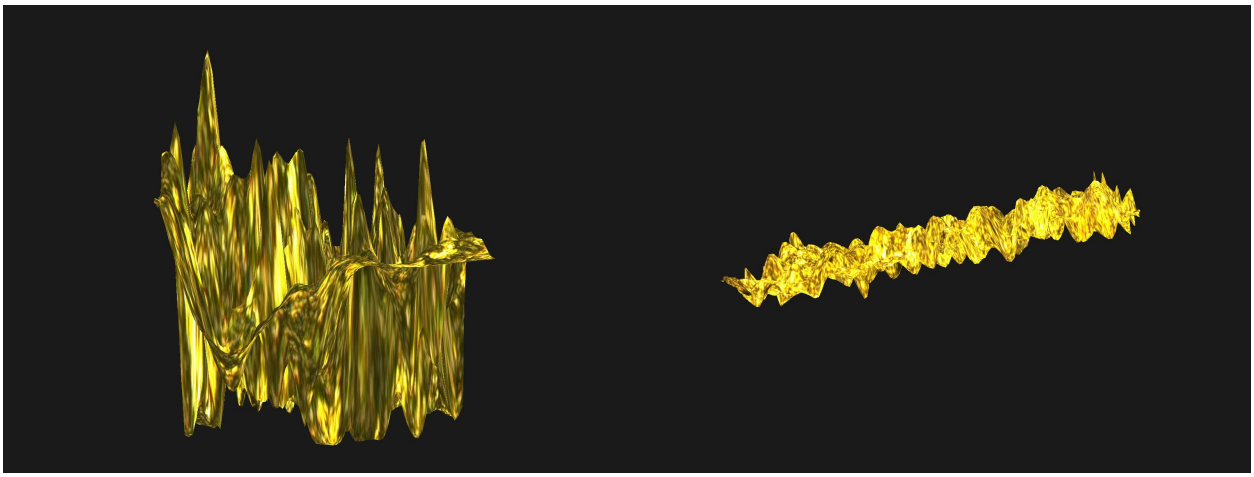

Figure 2.2: Surface Before Processing

Figure 2.3: Surface After Processing

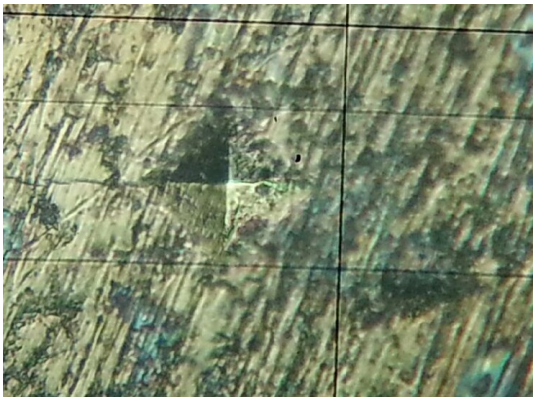

Figure 2.4: Hardness Test Indention in Terfenol-D Sample

Table 2.2: Hardness Test

Force Ranging			
Force (kg_f)	Microns	Vickers (kg_f/m^2)	HRC
0.3	26.9	768.7	62.8
0.5	38.4	628.7	56.7
1	57.2	566.7	53.3
Hardness Test			
Force (kg_f)	Microns	Vickers (kg_f/m^2)	HRC
0.5	34.3	788	63.5
0.5	34.9	761.2	62.5
0.5	34.2	792.7	63.7
0.5	34.2	792.7	63.7
0.5	34.8	765.6	62.7
Average			
Force (kg_f)	Microns	Vickers (kg_f/m^2)	HRC
0.5	34.48	780.04	63.22

2.2 Relative Permeability at No Load

To be able to calculate the relative permeability at different conditions, it is necessary to measure the permeability at no load. One way to attain this value is to create an inductor with Terfenol-D at its core, measure its inductance, model it using Finite Element Method Magnetics (femm), and change the relative permeability until the inductance values match the measured values. Washers made of stainless steel are affixed to either end of a Terfenol-D Core using a 5-minute epoxy creating a spindle. This spindle is then wound with 372 turns of size 30 AWG (American Wire Gauge)

enameled magnet wire. The resulting inductor is pictured in Figure 2.5. An LCR meter is used to measure the inductance with 1 kHz sampling frequency and 5% tolerance. The inductance of the spindle was found to be 3.610 mH. This fixture design will be referred to as the "washer-spool fixture". The electromagnetic behavior of this inductor is then modeled using the femm software. The dimensions of the fixture are measured and the properties of each material used are recorded. An arbitrary relative permeability is selected for Terfenol-D. The final femm model is shown in Figure 2.6. A mesh is then created with 4000 points and the model is simulated. The inductance is calculated by dividing the flux linkage by the current. After numerous simulations, each time adjusting the relative permeability until the inductance matches that of the physical model, the relative permeability was found to be ~3.705 H/m.

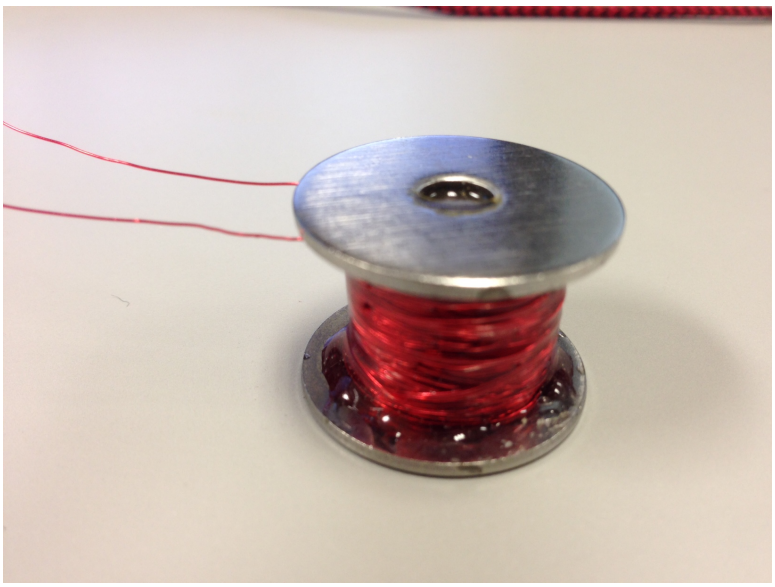

Figure 2.5: Terfenol-D Cored Inductor

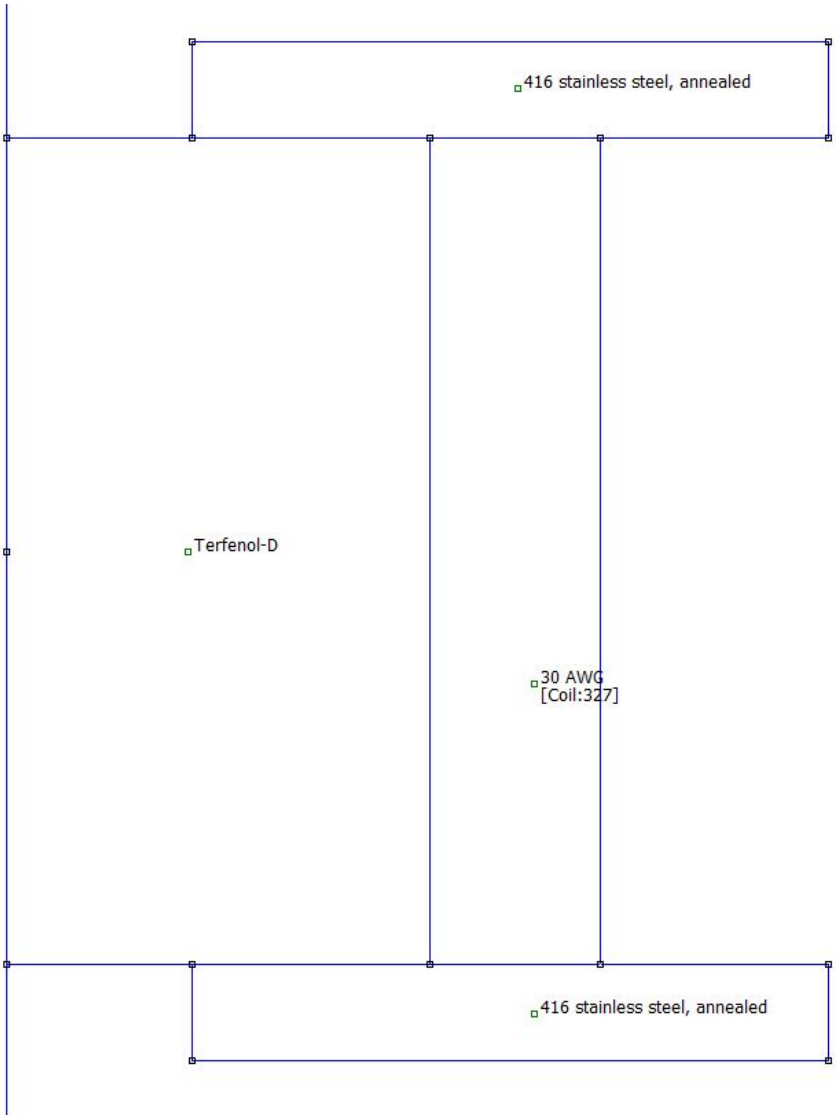

Figure 2.6: Terfenol-D Cored Inductor femm Model

2.3 Young's Modulus and Compressive Strength

Both Young's Modulus and the compressive strength of the Terfenol-D can be extracted by compressing the material and observing its response. Of particular interest is the relationship between stress and strain. The Material Test System (MTS) is used to compress the material. Hydraulics are used to control the position and the force of platens in the MTS accurately. Exerting a known force on the platens and observing the change in displacement, the material properties of various alloys and fixtures can be characterized. By raising the force applied to the fixture until it yields, the com-

pressive strength of the material as well as Young's Modulus can be determined. The compressive strength is the point at which the material yields; Most easily identified as where the slope of the stress/strain curve changes drastically, whereas, Young's Modulus is the slope of the stress/strain curve up to that point, i.e. the most linear part of the curve. The stress-strain curve obtained from the compression test is given in Figure 2.7.

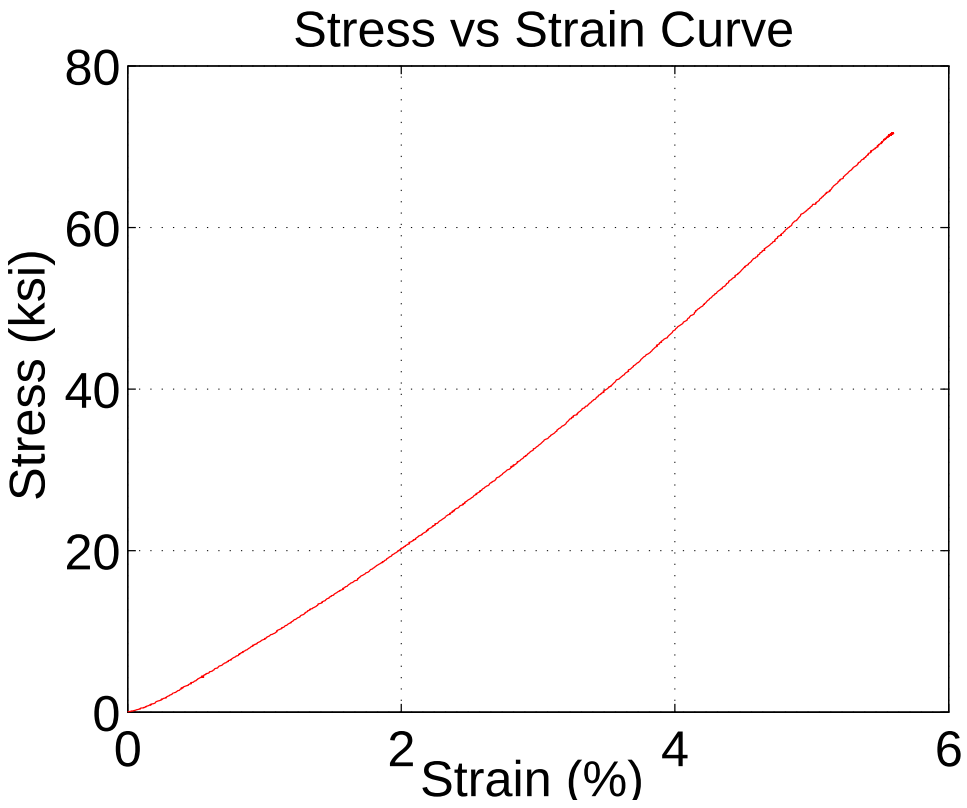

Figure 2.7: Compression Test - Stress vs Strain

A linear fit of the plot gives Young's Modulus as 22GPA. From the plot, it can be observed that the material did not yield. The range of forces used for the test exceed the maximum load expected for the largest dimensions for the final fixture. Even though the compressive strength can't be obtained until a yield point is reached, the material proved to be able to withstand the load during normal operation.

2.4 Software Interface

The LCR meter used throughout the design and testing of the sensor being developed came with its own proprietary software for recording inductance readings over time. Unfortunately, the measurements being recorded using this software did not have a consistent time between readings nor did they record timestamps. Attempting to use the meter in this state would result in inconsistent and incorrect readings of inductance for varying loads. To this end, a GUI (Graphical User Interface) was designed that records the inductance and associates it with the time of the computer running the script. MATLAB is chosen for this purpose as it has a built-in interactive toolbox for designing GUIs called GUIDE (Graphical User Interface Development Environment). The exact process for designing this GUI is explained in Appendix B.

The majority if of the testing that was conducted for characterization purposes was carried out using the MTS (Material Test System) pictured in Figure 0.20. The model that is available is equipped with two compression platens, which are rated for 276 MPa static load, which exceeds the pressure expected in this application. There are two methods of controlling the MTS: Manually using the controller depicted in Figure 0.21, or by using a Flex Test 40 Controller installed on a dedicated desktop computer. For the purpose of the sensor testing, the latter configuration will be utilized.

CHAPTER III.

FIXTURE DESIGN

In designing a fixture best suited for a particular application, it is impossible to foresee all the complications that will inevitably arise. As a result, the fixture design underwent numerous revisions, consistently improving the functionality and/or addressing any complications along the way. Each fixture was modeled both structurely using Solidworks and electromagnetically with femm. After which, the effectiveness of the new fixture was assessed. This process involved several iterations in order to achieve optimal performance. Design changes include both revisions to the dimensions of the fixture as well as material selection as deemed necessary. Materials chosen be strong enough to withstand the forces present in service conditions, and must also be electromagnetically favorable for the fields generated during operation.

3.1 Washer-spool fixture

The simple "washer-spool fixture" created for the purpose of obtaining the relative magnetic permeability of the material is used as a baseline for improving the design. This fixture consists of washers affixed to either end of the Terfenol-D core forming a spool. That spool is then wound 280 times with size 30 AWG enameled magnet wire. A picture showing the assembly of this particular fixture can be seen in Figure 3.1. The physical and electromagnetic models are shown in Figure 3.2 and Figure 3.3, respectively. This configuration underwent cyclical loading from 0 to 500 lbf to verify its effectiveness in an environment where the load varies. Throughout the experiment, the amount of force necessary to compress the material appeared to change in each individual stroke (indicating hysteresis), and from cycle to cycle (indicating creep). In an attempt to identify the cause of the hysteresis and possible deformation, multiple cycle fast load experiments were performed. These experiments revealed that the fixture was deforming through the numerous

cycles. However, any deformation the fixture suffered was reversed within a couple of hours under no load. The "creep", as it is commonly referred to, is depicted in Figure 3.4. After reviewing the resulting plots, it is clear that the mechanical hysteresis present in the fixture is non-existent within the Terfenol-D rod, rather it must reside in either the washers or the epoxy used to hold the fixture together.

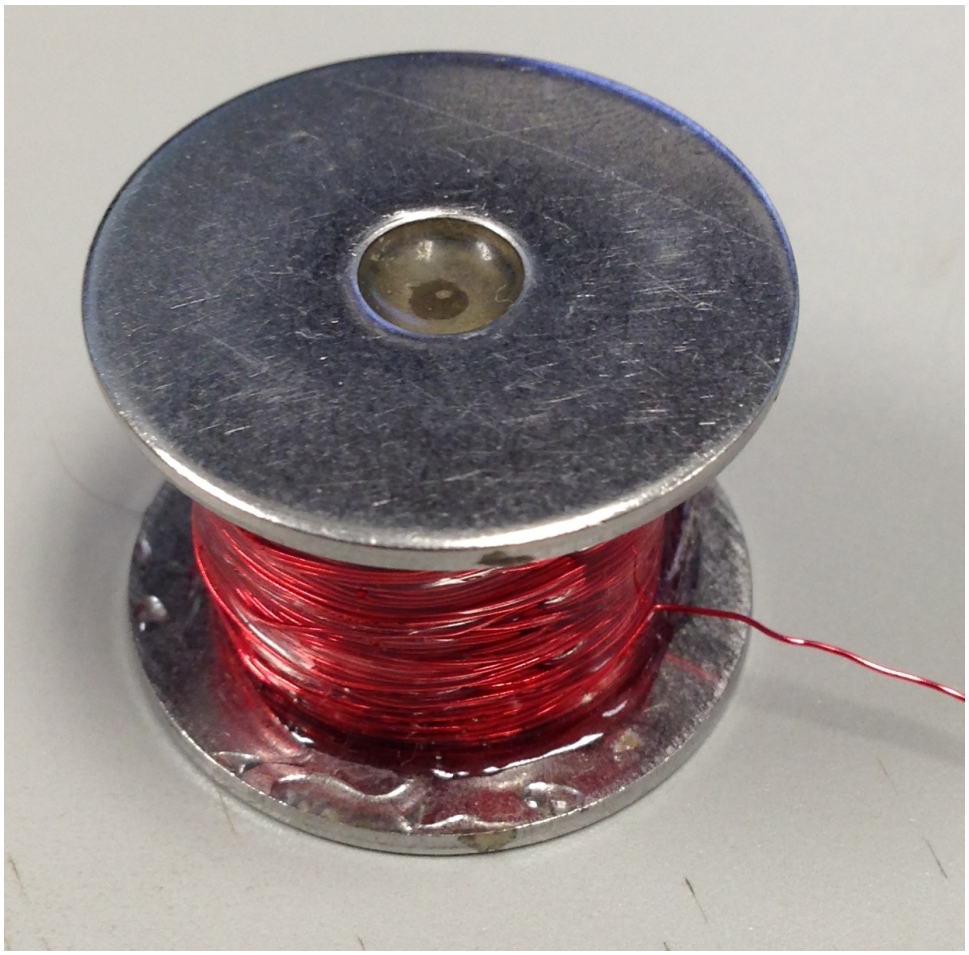

Figure 3.1: Washer-Spool Fixture

Figure 3.2: Washer-Spool Model Physical Model

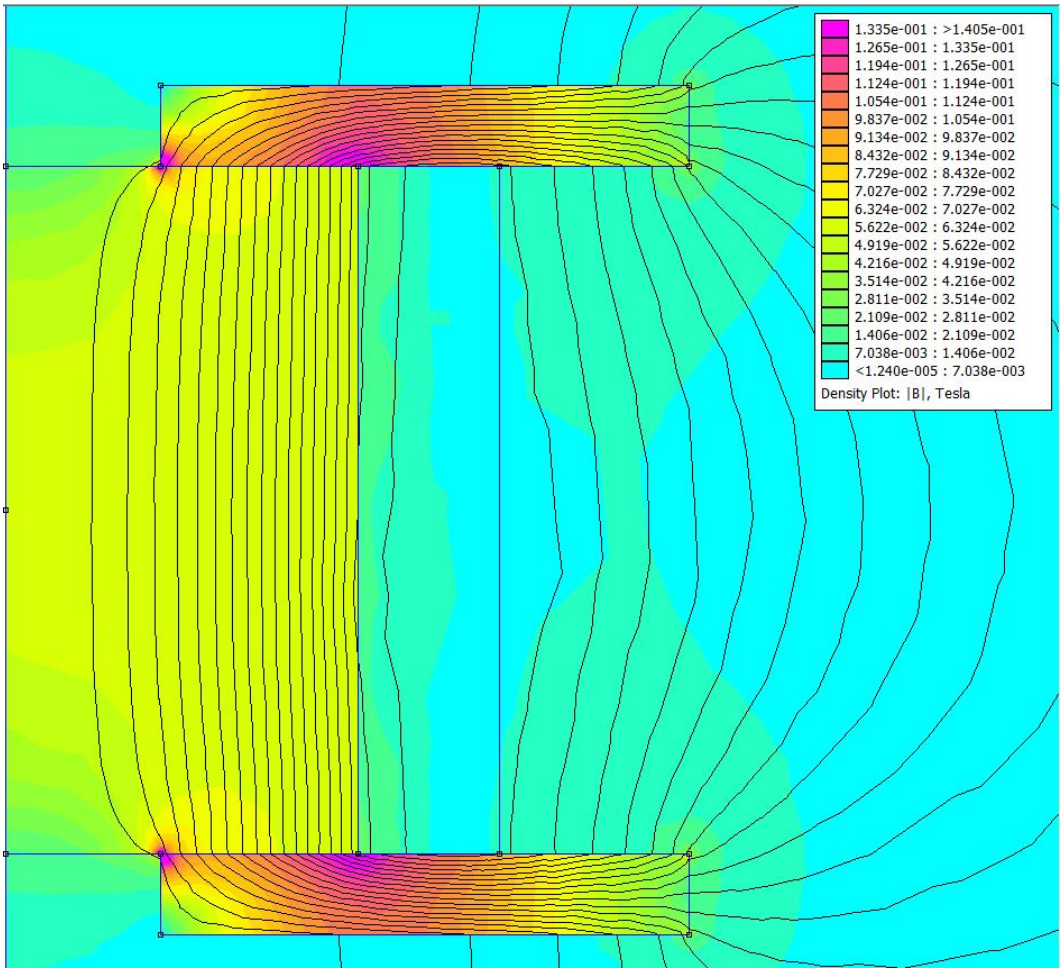

Figure 3.3: Flux Density Plot

After verifying the relationship between the load and displacement changes over time, the next step is to identify the part of the fixture this deformation is occurring. This can be achieved by conducting high cycle experiments with the different components of the fixture. The logical place to start is by testing the Terfenol-D rod. The same 1000 cycle experiment is applied to both the fixture without magnets and the blank Terfenol-D rod. The results are shown in Figure 3.5 and Figure 3.6.

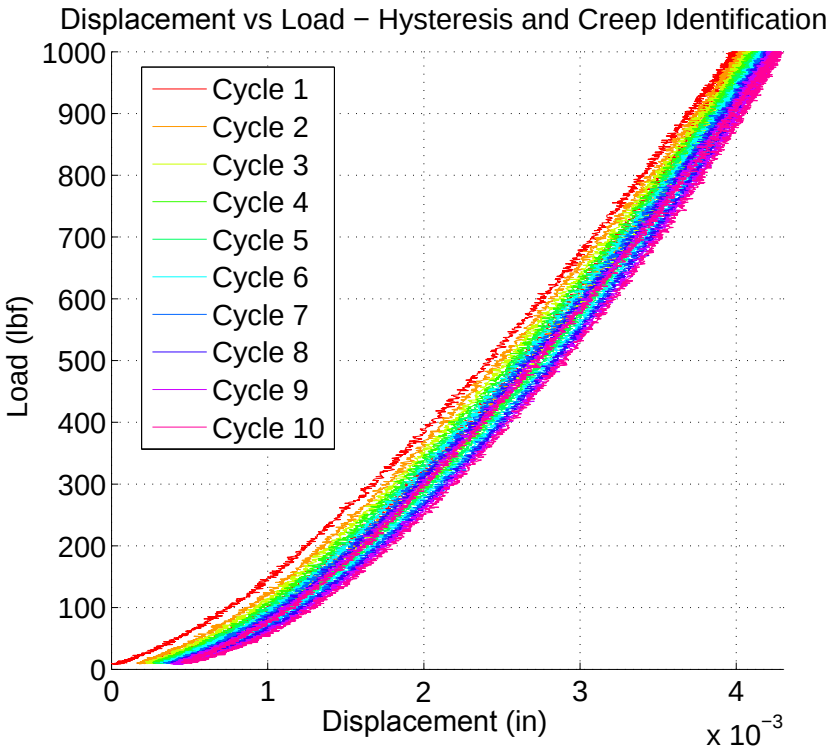

Figure 3.4: Hysteresis and Creep Identification

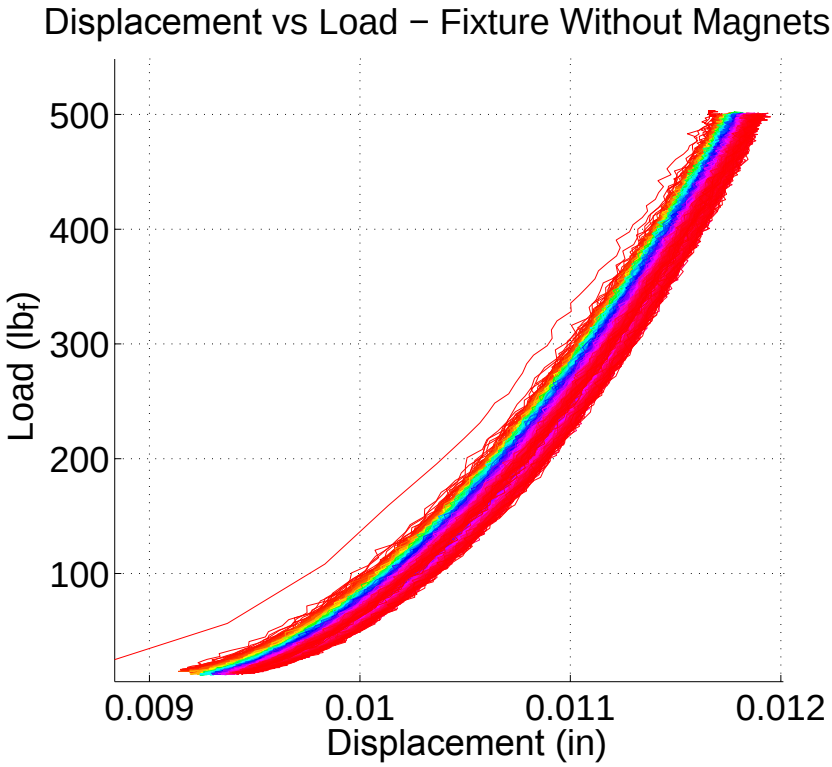

Figure 3.5: Compression Test - Fixture Without Magnets

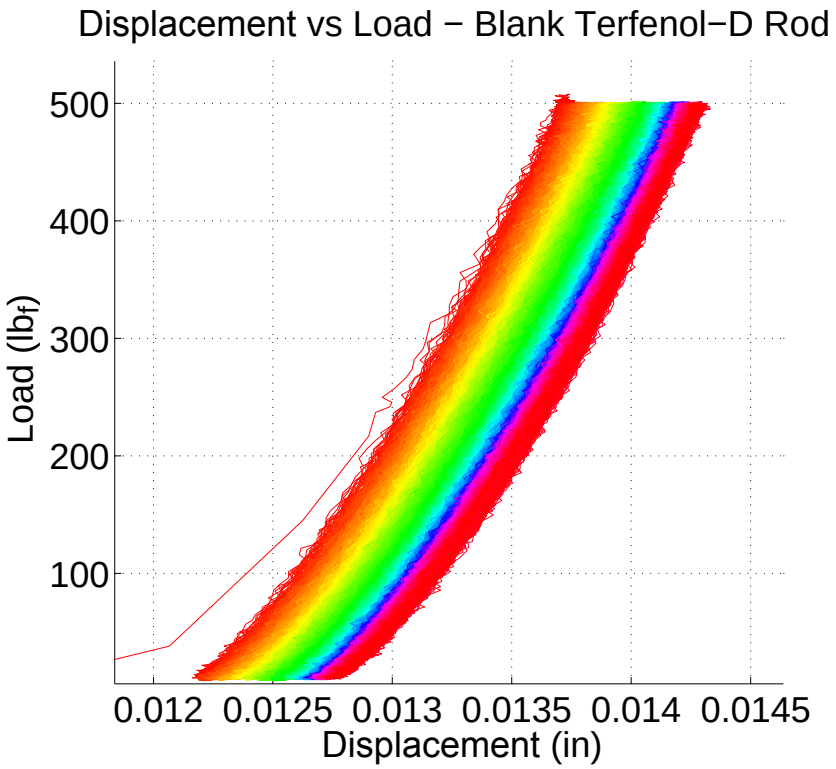

Figure 3.6: Compression Test - Blank Terfenol-D Rod

From the results, it appears as though both the deformation and creep are present in the Terfenol-D rod. To further investigate the creep, the sample is put through extensive testing and the height of the rod is measured after each test. All of the measurements yielded the exact same height (.500"). The latter result leads to the conclusion that the range in which the material is being loaded is still in the elastic region, that is, the material is not being permanently deformed. That conclusion does not seem plausible given the information shown in Figure 3.5 and Figure 3.6, therefore, the issue must be in the setup. Upon further inspection of the MTS, it was observed that the platens that are used for compression were not perfectly parallel, which caused the platens during cyclical testing can cause the sample to shift towards a section where the platens are wider, thus creating the illusion of deformation.

To address the aforementioned issue, an auto-leveling platen was used for all experiments from that point on. The auto-leveling platen consists of a stationary base with a round indention and a platen top with a greased ball that sits in that indention. The perimeter of the upper section

surrounded by springs to maintain an even level. When a load is centered on the platen, the ball in the socket will shift to maintain evenly distributed pressure; this in combination with the parallel surfaces of the fixture prevents any shifting. A picture of the auto-leveling platen is presented in Figure 3.7. As an additional countermeasure to the shifting of the fixture, the force was kept above 50 lbf during cyclical testing. This ensures there is no point in which the sample is not in contact with both platens. Cyclical loading is performed with the force ranging from 50 to 2000 lbf to verify the effectiveness of the implemented changes. The resulting displacement vs load plot is shown in Figure 3.8.

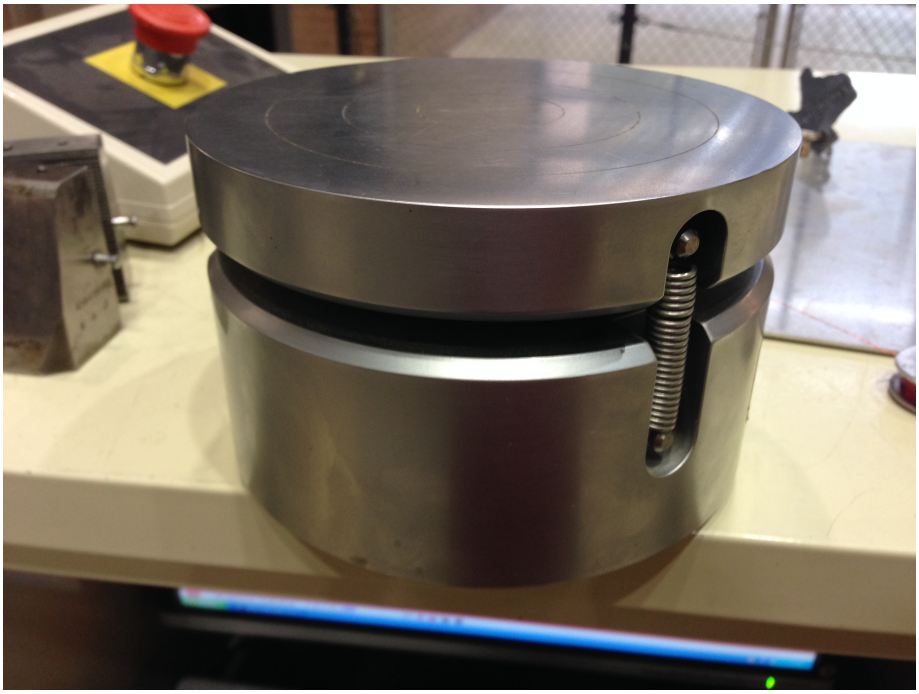

Figure 3.7: Auto-Leveling Platen Fixture

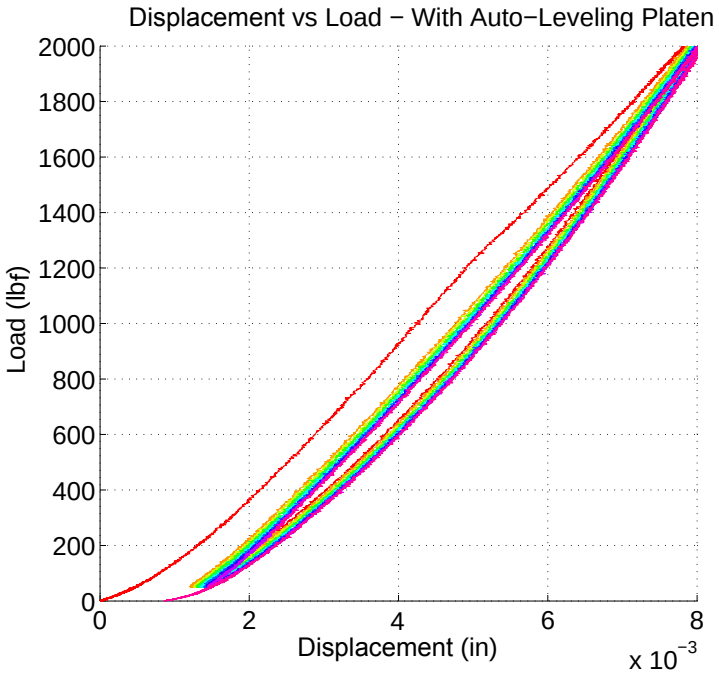

Figure 3.8: Compression Test - Auto-Leveling Platen

Comparison of the resulting plot with Figure 3.4 shows considerably less creep. The hysteresis persists even after the implementation of an auto-leveling platen; therefore, it can be deduced that the source of the hysteresis is in the Terfenol-D core itself. To test this, an experiment is conducted with both the blank Terfenol-D rod and the "washer-spool" fixture. Both of which showed similar hysteresis curves, supporting the statement that the hysteresis is present only in the Terfenol-D rod.

3.2 Stainless Steel Spool Fixture

The electromagnetic model of the previous fixture indicates a significant amount of the electromagnetic field is being diverted into the washers placed at either end causing the fixture to behave differently on different surfaces. To remedy this, the washers must be made of a material that is nonmagnetic. Several materials were considered, the first of which is plastic. Spools were created from within the dimensions required; however, they proved to be too malleable and difficult to machine. A rigid material is required for this application. The washers chosen for this new fixture are made of 316 stainless steel. These washers have a maximum relative magnetic permeability of

~1.005, which is close to that of air. The closer the magnets are to the core, the greater the magnetic field through the Terfenol-D is, thereby generating more energy. For this reason, the washer dimensions are selected such that the Terfenol-D core may fit inside the inner diameter.

From the physical model of the previous fixture, it is clear that a fraction of the force being applied to the washers is supported by the wire coils. The latter is undesirable as it reduces the force applied to the Terfenol-D core in an unpredictable manner. The fixture is designed such that the only part being compressed is the Terfenol-D core. The latter is achieved by placing the washers around the perimeter of the Terfenol-D and having them slightly offset from the ends of the rod. A visual representation of this fixture and all its components is provided in Figure 3.10.

A magnetic model for the fixture is presented in Figure 3.11. The flux density plot illustrates the magnetic field generated by the magnets is unimpeded by the washers, which allows for simpler calculations when determining the flux of the path along which the field is focused. The spool of this fixture is wound 390 times with size 30 AWG enameled magnet wire, resulting in a base inductance of 4.25 mH. This notably higher than the previous fixture, however, will not be an issue as the relationship between the force and the permeability remains unchanged.

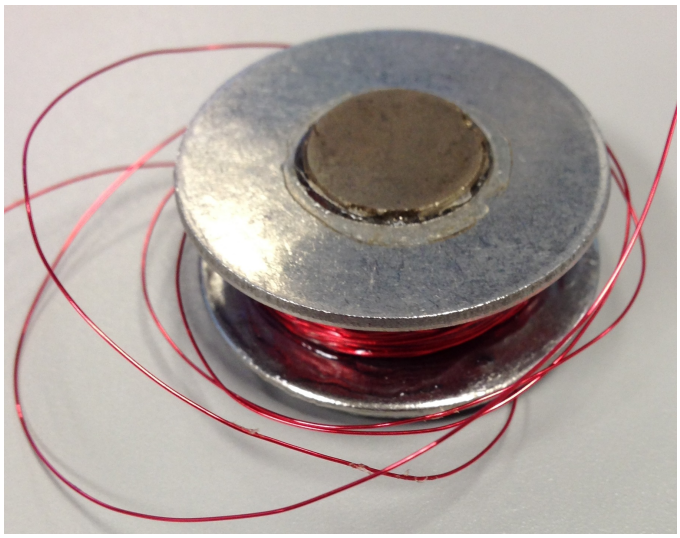

Figure 3.9: Stainless Steel Spool Fixture

Figure 3.10: 316 Stainless Steel Spool Physical Model

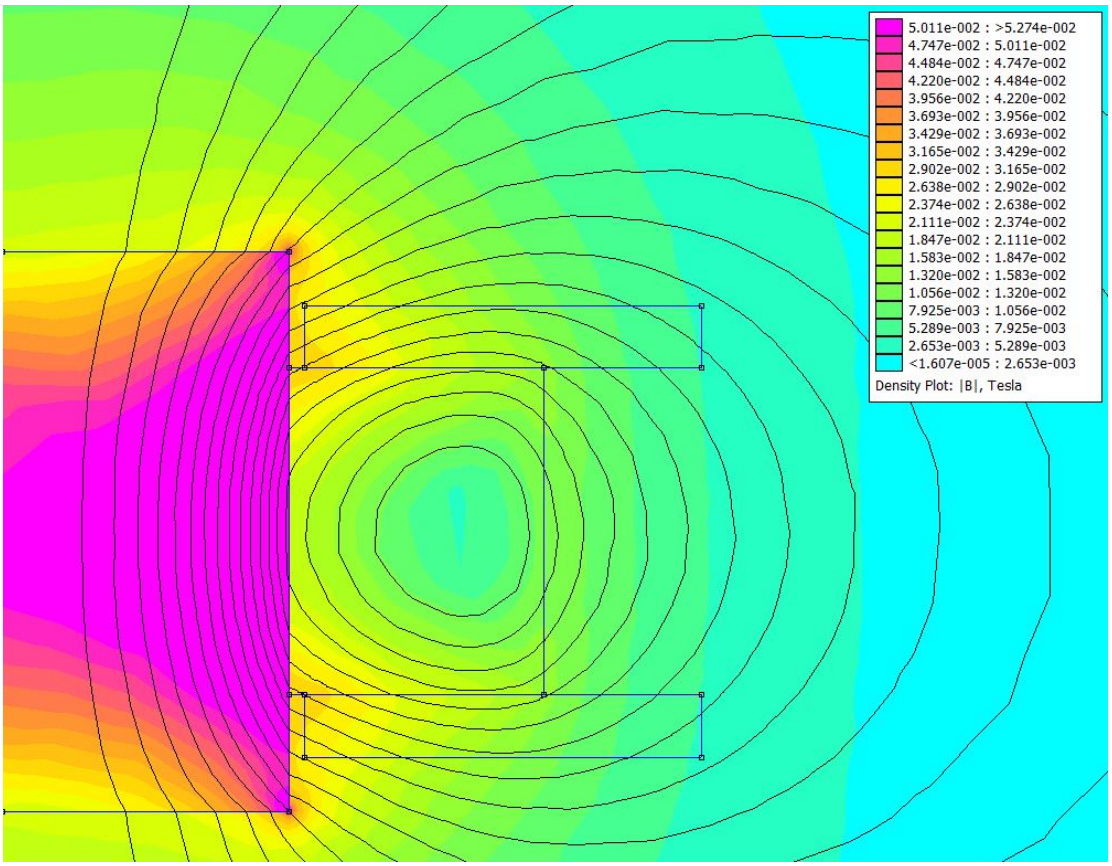

Figure 3.11: Flux Density Plot for 316 Stainless Steel Spool Fixture

3.3 Magnetic Field Insulating Fixture

Much of the magnetic field inside the Terfenol-D is dependent on its environment. Predictability of response is a requirement for any well-calibrated sensor. A fixture change is necessary so that the sensor behaves in a ascertainable manner, which was achieved by enclosing the magnetic field inside the fixture. For this purpose, 1018 steel was chosen as it is both durable and highly magnetic (i.e. has a high relative permeability). Soft magnetic materials have a permeability that changes with the strength of the applied field. The relative permeability for 1018 steel over a range of fields is listed in Table 3.1. Magnetic fields at the surface of the fixture range from .2 to .55 Tesla. The relative permeability can be interpolated from Table 3.1 using a cubic spline and a shape preserving interpolation. For the range of field strengths given, the relative permeability expected is from 800-950, which is more than enough to direct the magnetic field in this application. This statement

is corroborated by the electromagnetic model of the assembled fixture depicted in Figure 3.14.

Damage of the Terfenol-D rods caused by lateral force is a major concern. An example of this wear is shown in Figure 3.12. Terfenol-D was chosen for its durability in the y-axis; however, its crystal alignment causes it to be very fragile in any other axis. The changes implemented in this fixture revision aim to minimize lateral forces applied to the Terfenol-D core by limiting the range of motion in that direction. An actuating piston is set in a ring, such that it can only move along the y-axis. The Terfenol-D rods were all damaged during the initial testing phase. New samples were ordered that are slightly longer 1.905 cm (.75 in) than the orginal ones which were 1.27 cm (.5 in), thus, allowing more windings closer to the core. The physical model of this fixture is rendered in Figure 3.13. A picture of this fully-assembled fixture is presented in Figure 3.15.

Table 3.1: Relative Permeability of 1018 Steel

Steel 1018	
$B\ (tesla)$	μ_R
0.0000	790.6271
0.2500	833.4465
0.9250	924.9707
1.2500	624.9802
1.3900	463.3380
1.5250	304.9980
1.7100	170.9989

Figure 3.12: Terfenol-D Wear and Tear Caused by Lateral Loading

ITEM NO.	PART NAME	DESCRIPTION	QTY.
1	Rod	1018 Steel	1
2	Notched Ring	1018 Steel	1
3	Terfenol	$Tb_3Dy_7Fe_2$	1
4	Spool	Aluminum	1
5	Coil	Magnet Wire: size 26 AWG, 200 turns	1
6	Washer-.075"	Aluminum	1
7	Base	1018 Steel	1

PROPRIETARY AND CONFIDENTIAL

THE INFORMATION CONTAINED IN THIS DRAWING IS THE SOLE PROPERTY OF <INSERT COMPANY NAME HERE>. ANY REPRODUCTION IN PART OR AS A WHOLE WITHOUT THE WRITTEN PERMISSION OF <INSERT COMPANY NAME HERE> IS PROHIBITED.

UNLESS OTHERWISE SPECIFIED:

DIMENSIONS ARE IN INCHES
TOLERANCES:
FRACTIONAL ±
ANGULAR: MACH ± BEND ±
TWO PLACE DECIMAL ±
THREE PLACE DECIMAL ±

INTERPRET GEOMETRIC TOLERANCING PER:

MATERIAL

FINISH

DO NOT SCALE DRAWING

	NAME	DATE
DRAWN		
CHECKED		
ENG APPR.		
MFG APPR.		
Q.A.		
COMMENTS:		

APPLICATION

USED ON

NEXT ASSY

TITLE:

Magnetic Field Insulating Fixture Short Assembly

SIZE	DWG. NO.	REV
A		
SCALE: 1:1	WEIGHT:	SHEET 1 OF 1

Figure 3.13: Magnetic Field Insulating Fixture Physical Model

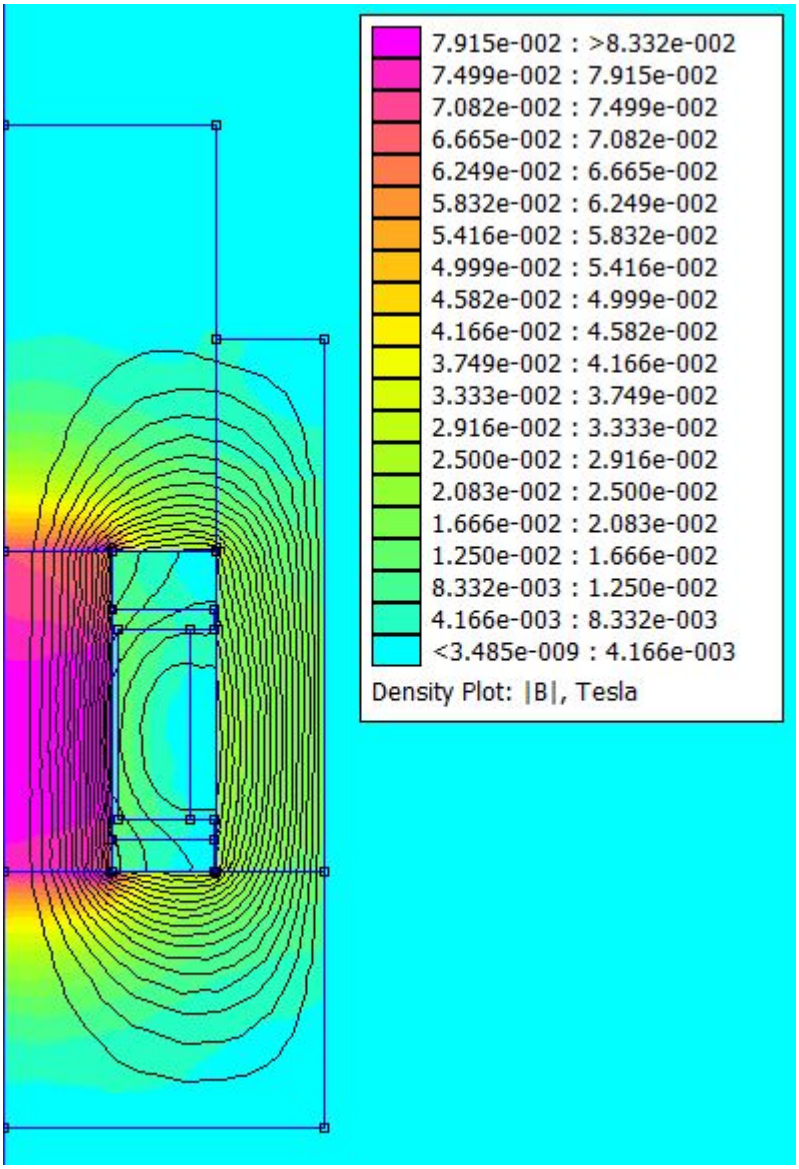

Figure 3.14: Flux Density Plot for Magnetic Field Insulating Fixture

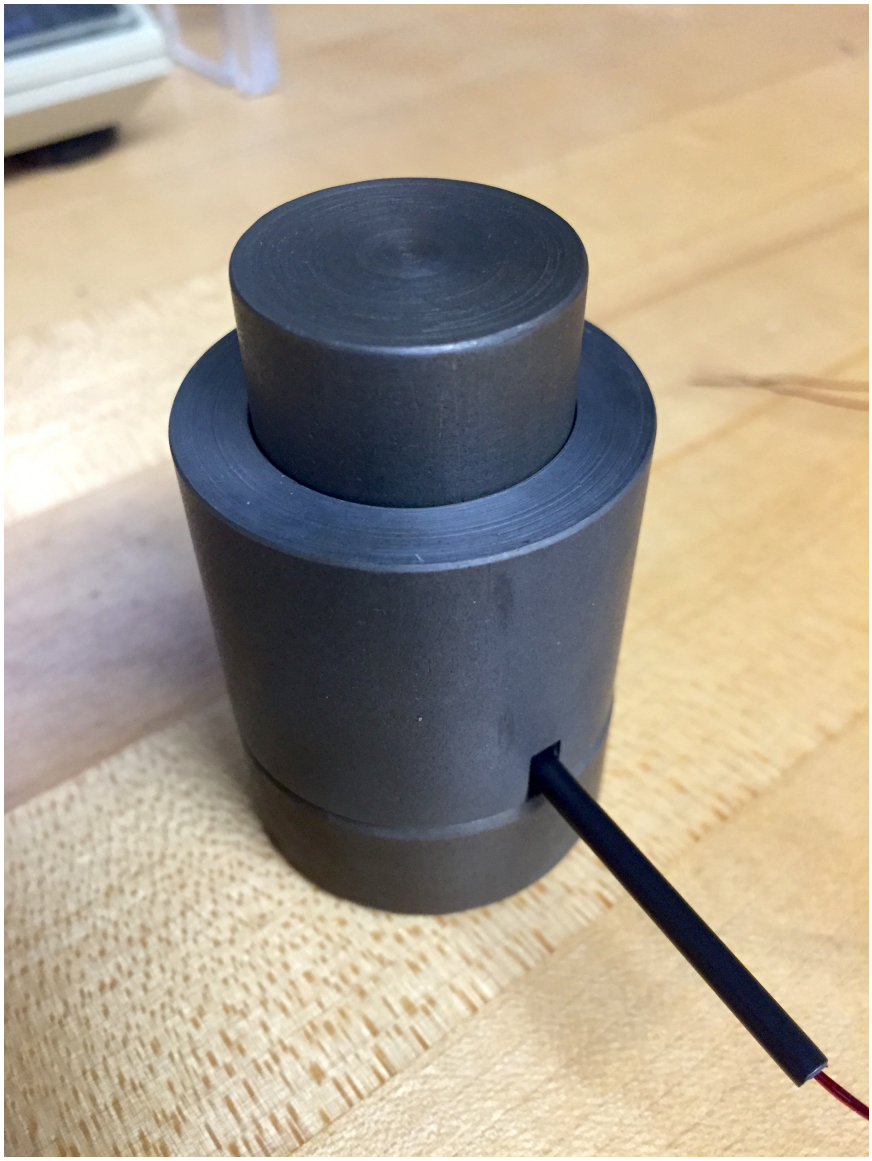

Figure 3.15: Assembled Magnetic Field Insulating Fixture

The flux density plot depicted in Figure 3.14 suggests that this fixture is more than sufficient to confine the magnetic field to the Terfenol-D core. The relationship between load and displacement is improved when compared to the bare Terfenol-D sample, thus, making this iteration of the fixture design more optimal. The creep is also lessened, which can be attributed to the increased surface area of the fixture making contact with the tester. The plot of displacement vs load is shown in Figure 3.16.

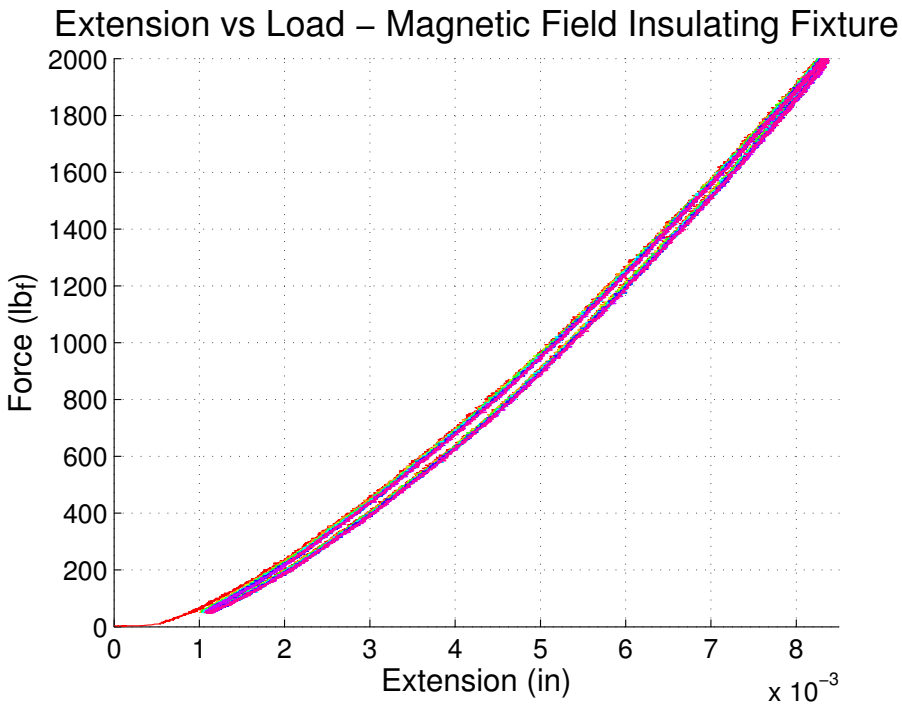

Figure 3.16: Compression Test - Magnetic Field Insulating Fixture

3.4 Modified Magnetic Field Insulating Fixture

The magnetic field insulating fixture, while useful for load sensing, is not designed in accordance to the requirements for energy harvesting. The limiting factor being, that it is not physically capable of housing the Terfenol-D and the two magnets necessary for power generation. The latter was addressed by raising the height of the notched ring and the rod. The physical and magnetic models are pictured in Figure 3.17 and Figure 3.18, respectively.

ITEM NO.	PART NAME	DESCRIPTION	QTY.
1	Rod	1018 Steel	1
2	Notched Ring	1018 Steel	1
3	Terfenol	$Tb_3Dy_7Fe_2$	1
4	Spool	Aluminum	1
5	Coil	Magnet Wire: size 26 AWG, 200 turns	1
6	Washer-.075"	Aluminum	1
7	Base	1018 Steel	1

PROPRIETARY AND CONFIDENTIAL

THE INFORMATION CONTAINED IN THIS DRAWING IS THE SOLE PROPERTY OF <INSERT COMPANY NAME HERE>. ANY REPRODUCTION IN PART OR AS A WHOLE WITHOUT THE WRITTEN PERMISSION OF <INSERT COMPANY NAME HERE> IS PROHIBITED.

UNLESS OTHERWISE SPECIFIED:
DIMENSIONS ARE IN INCHES
TOLERANCES:
FRACTIONAL ±
ANGULAR: MACH ± BEND ±
TWO PLACE DECIMAL ±
THREE PLACE DECIMAL ±
INTERPRET GEOMETRIC TOLERANCING PER:
MATERIAL
FINISH
NEXT ASSY
USED ON
APPLICATION
DO NOT SCALE DRAWING

	NAME	DATE
DRAWN		
CHECKED		
ENG APPR.		
MFG APPR.		
Q.A.		
COMMENTS:		

TITLE:
Magnetic Field Insulating Fixture Short Assembly

SIZE A | DWG. NO. | REV
SCALE: 1:1 | WEIGHT: | SHEET 1 OF 1

Figure 3.17: Physical Model of the Magnetic Field Insulating Fixture

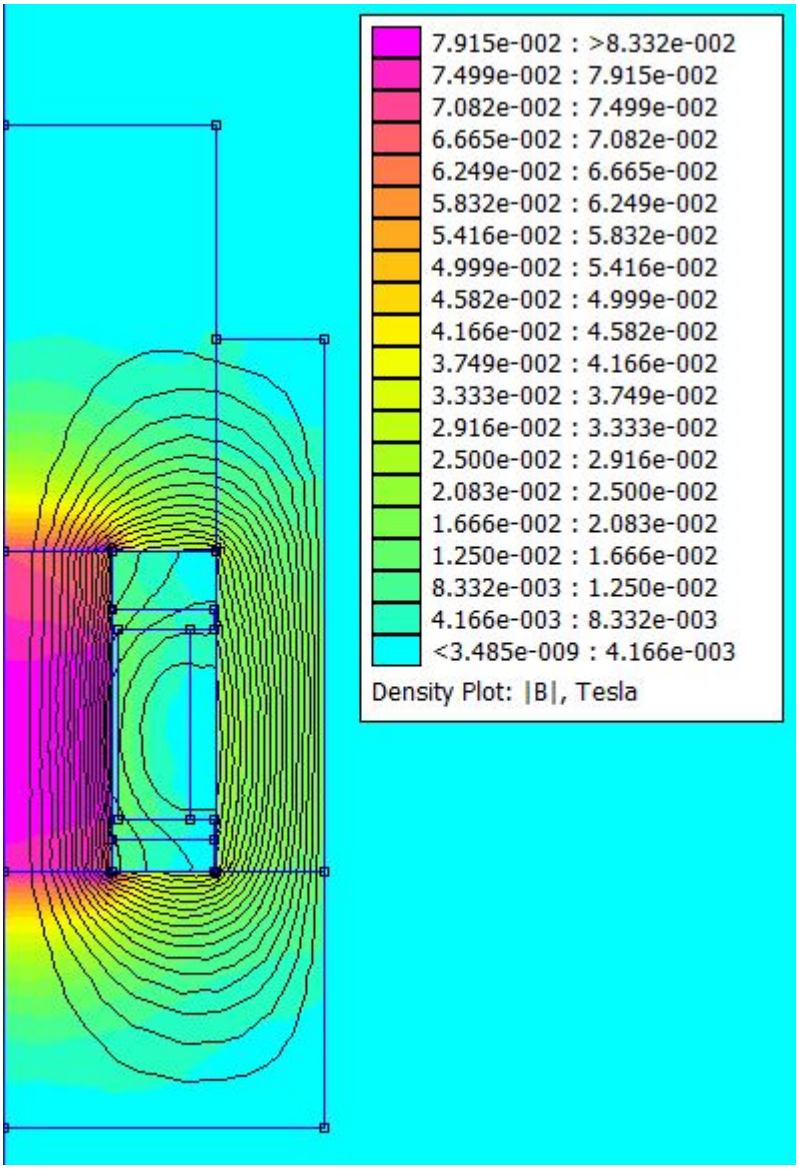

Figure 3.18: Flux Density Plot for Magnetic Field Insulating Fixture

3.5 Aluminum Spools

The wear and tear sustained by the Terfenol-D in testing made it necessary to create a separate spool to maintain consistency in inductances across different experiments. Initially, plastic was chosen for this task due to its flexibility and relative permeability being close to 1. Unfortunately, plastic is difficult to machine without deformation. An example of the deformation that occurs is shown in Figure 3.19.

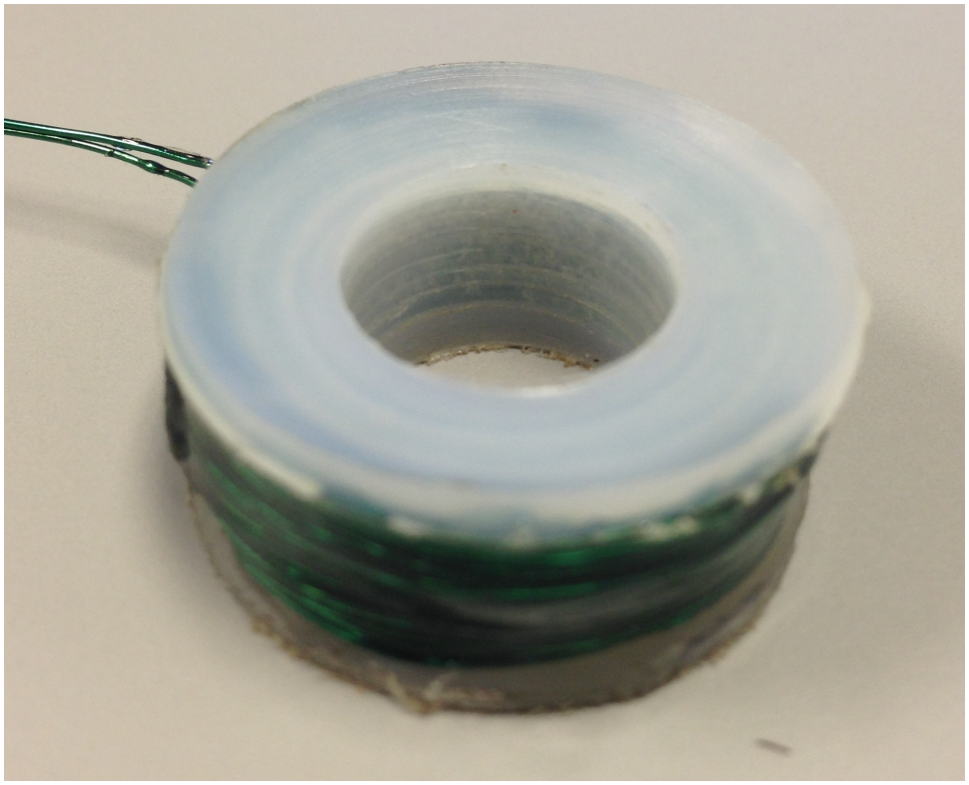

Figure 3.19: Plastic Spool Deformation

To promote durability, consistency, and ease of machining, aluminum was chosen as the material for the spool. Two spools of different heights were designed and fabricated. The first is 1.37 cm (.54 in) high and is short enough to allow ample compression of the core for load sensing experiments. The second is 1.905 cm (.75 in) high to allow for maximum number of turns around the Terfenol-D core, and is intended for energy harvesting experiments. Several aluminum washers of various sizes were machined to keep the spool centered around the Terfenol-D rod when these spools are utilized. The magnet wire used for previous fixtures was a low gauge to allow for more turns; unfortunately, this led to many of the spools becoming unusable when the wires broke. Hence, size 26 AWG was chosen for durability in testing. The physical models for the short and tall spools are given in Figure 3.20 and Figure 3.21, respectively. A picture of the assembled spools is depicted in Figure 3.22.

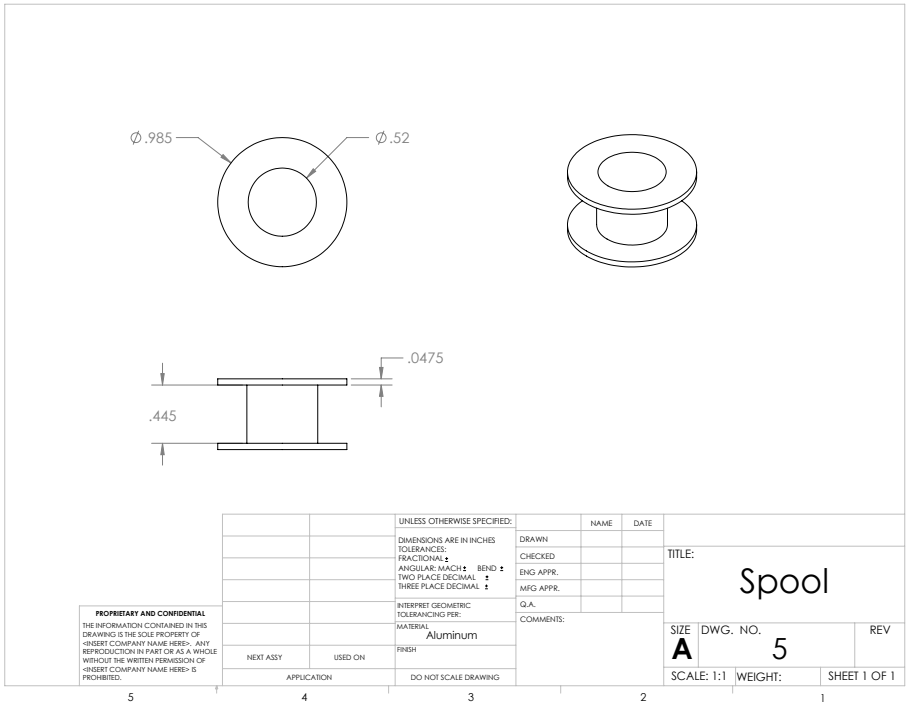

Figure 3.20: Short Aluminum Spool

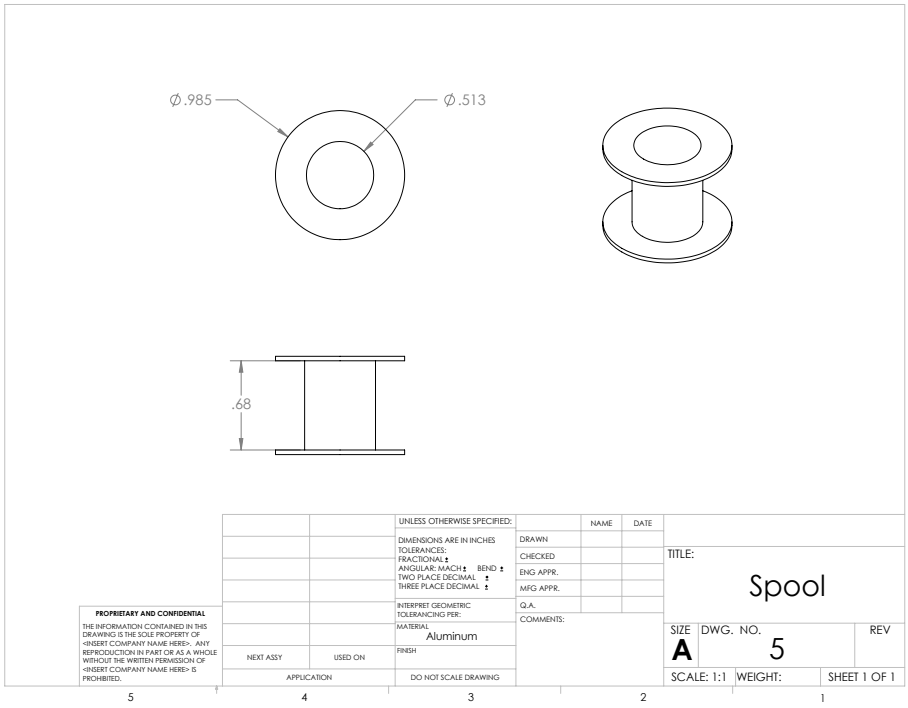

Figure 3.21: Tall Aluminum Spool

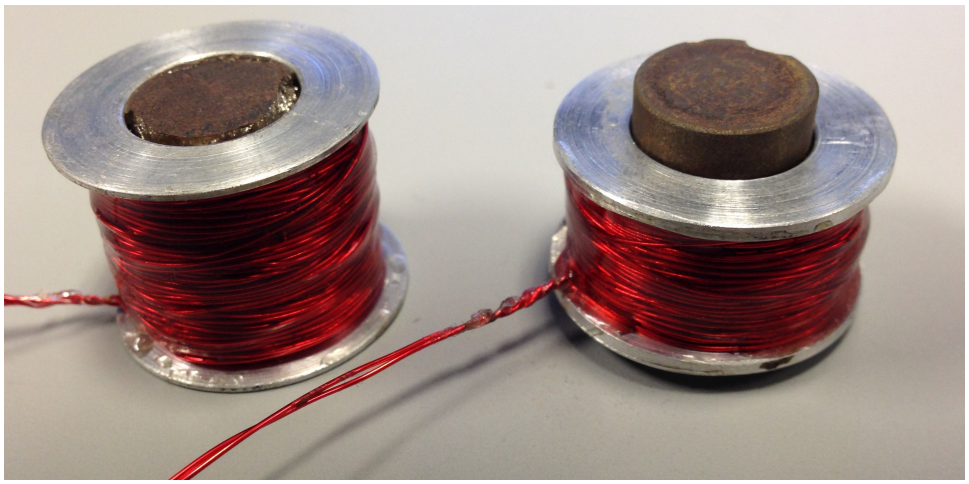

Figure 3.22: Wound Aluminum Spools

CHAPTER IV.

LOAD SENSOR CHARACTERIZATION

Having the ability to reliably determine the load and its distribution is an integral part of railcar monitoring systems. Generally, load distribution is measured through the use of load cells, transducers that convert a force into an electrical signal. The force in a particular direction deforms a strain gage that changes the resistivity of the wire. This change in resistivity is then measured by sending an electrical signal through it and observing the output. Load cells are placed along the tracks on weigh-in stations, where the train comes to a complete stop and the load distribution is measured. Some sensors have been improved such that the train need not come to a full stop. Standard installation of these sensors is illustrated in Figure 4.1. While very useful, these types of sensors do not constitute a true real-time monitoring system. To monitor the load in real-time during normal operation, new onboard monitoring technologies are being developed and tested. It is the goal of this project to create a sensor capable of providing load measurements with sufficient accuracy to be considered a feasible alternative to these load sensors. To this end, experiments conducted on the Terfenol-D based sensor are designed using the same range of pressures that the load cells are exposed to under normal operation.

Figure 4.1: Load Cells in the Rail

4.1 Load Range Calculation

Pressure film studies were conducted to show the distribution of load over the bearing adapter. The results of these studies at 50% and 100% load are shown in Figure 4.2. From the figure legend, the pressure exerted on the pad ranges from a minimum of 0 psi (no contact at all) to a maximum of about 1400 psi. The average pressure that the Terfenol-D sensor needs to withstand under maximum load is used to calculate the load range. The relationship between pressure and force is $p = F/A$, where p is the pressure, F is the force, and A is the surface area. Using the cross-sectional area of the widest point in the fixture, it is then possible to calculate the range of forces that will be used for testing:

$$F = pA \tag{4.1}$$

$$= (600\ \ psi)(\pi r^2) \tag{4.2}$$

$$= (600\ \ psi)(\pi(1in)^2) \tag{4.3}$$

$$\approx 1885\ \ lb_f \tag{4.4}$$

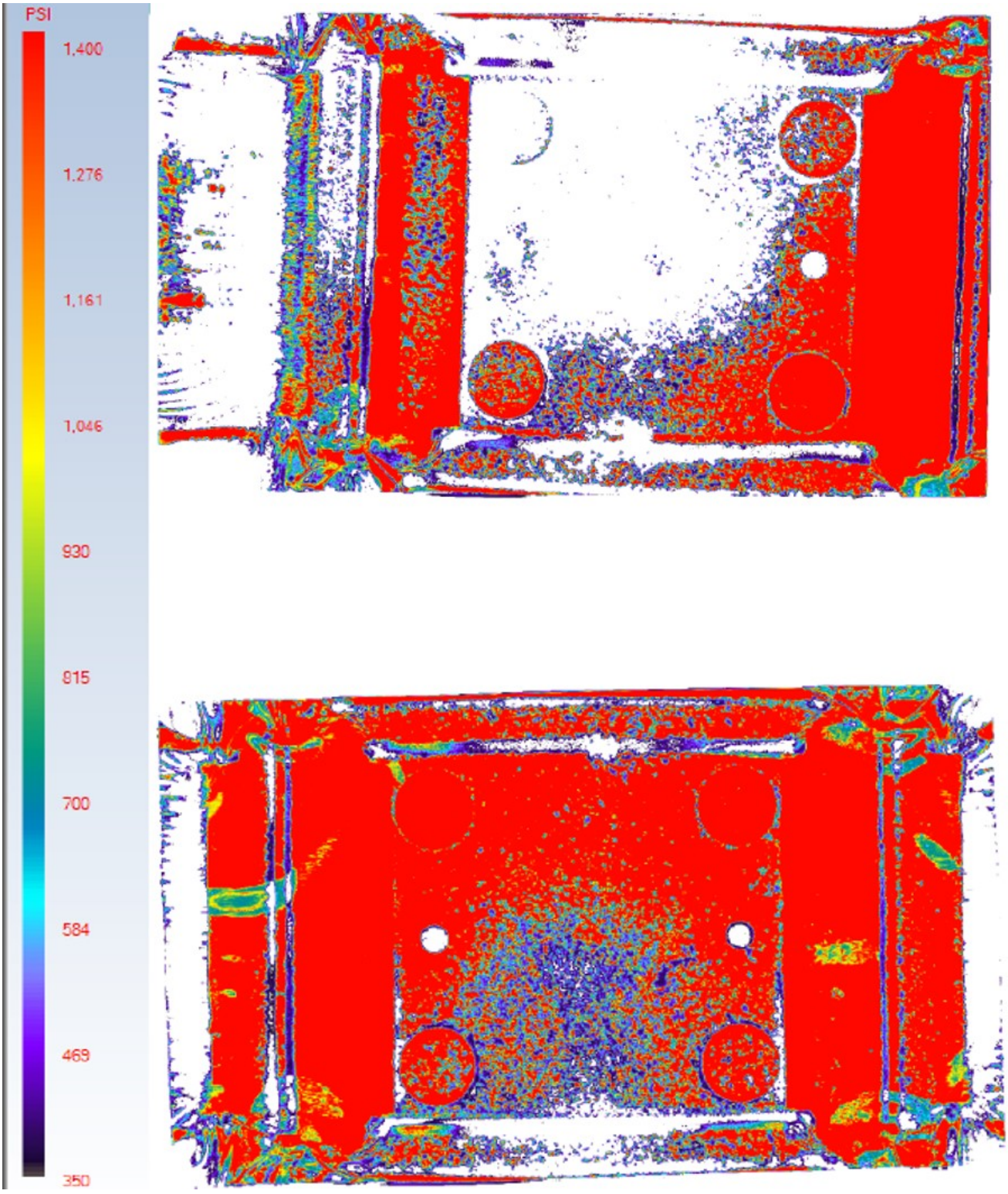

Figure 4.2: Pesudocolor Representation of Pressure at 50% and 100% load

4.2 Initial Load Testing

The relationship between the applied load in the z-axis and the inductance of the fixture was characterized through a set of experiments. These tests consisted of a varying load cycling between 0 and 1000 lb_f at intervals of 50 lb. The load was manually controlled while the inductance was measured at each point after settling. The results, displayed in Figure 4.3, show consistency. To function as a static load sensor, the response needs to be predictable at any given load, which is not possible in its current configuration due to the hysteresis present in Figure 4.3. For this reason, steps are taken to remove hysteresis.

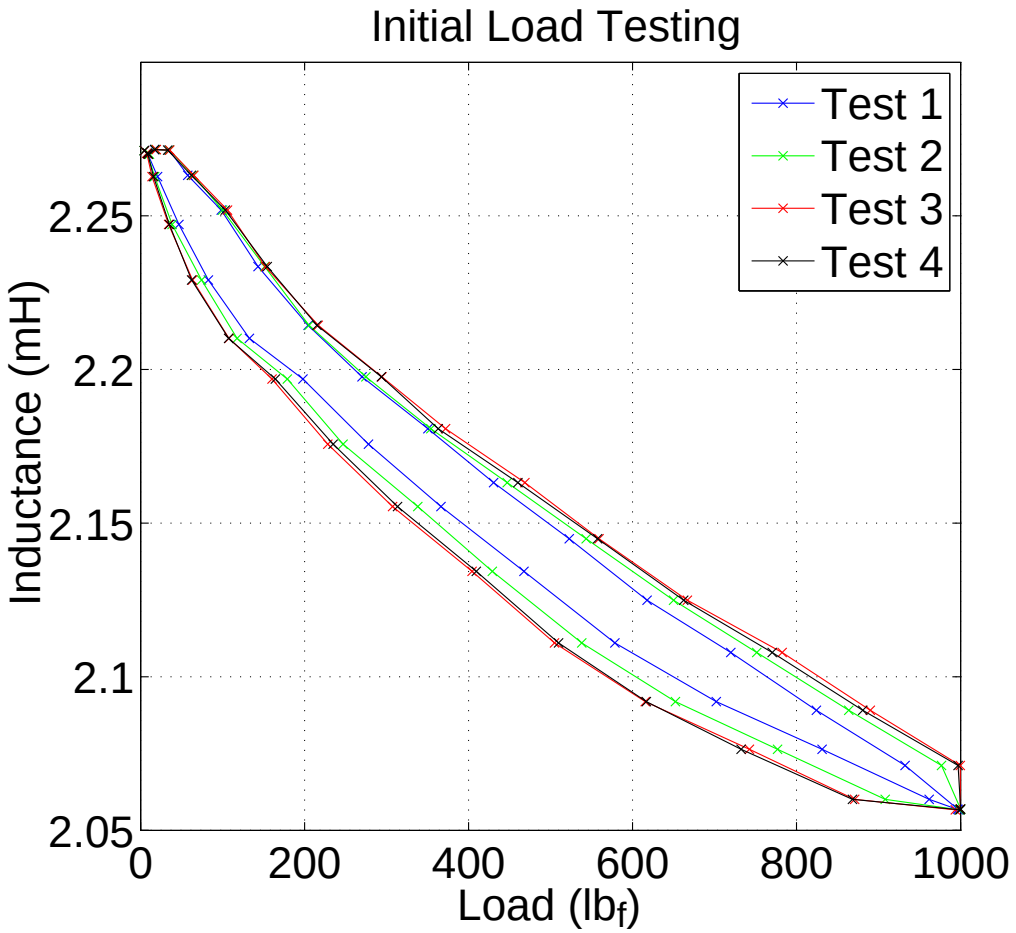

Figure 4.3: Initial Load Test

4.3 Varying Load and Speed

Before any improvements can be made, it is necessary to determine how the sensor will perform under various operating conditions. Multiple experiments of varying loads and speeds were performed to determine what effect these changes would have on the relationship between inductance and load. The load profiles that were utilized in these experiments are shown in Figure 4.4 and Figure 4.5. The results of these experiments are presented in Figure 4.6. The coil used for testing was damaged beyond repair. For this reason, a lower turn coil using higher gauge magnet wire was used for all future testing.

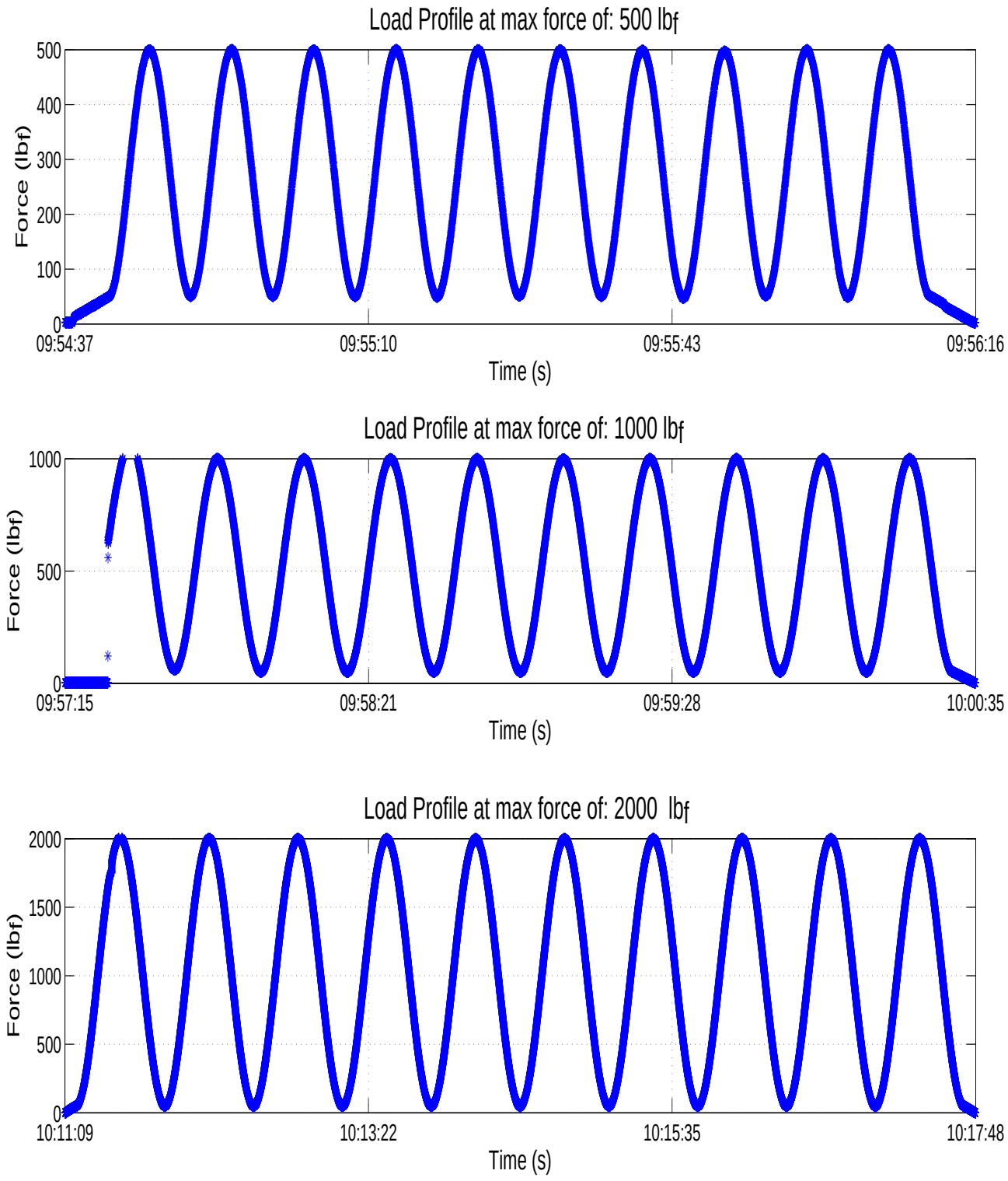

Figure 4.4: Varying Maximum Load Profiles

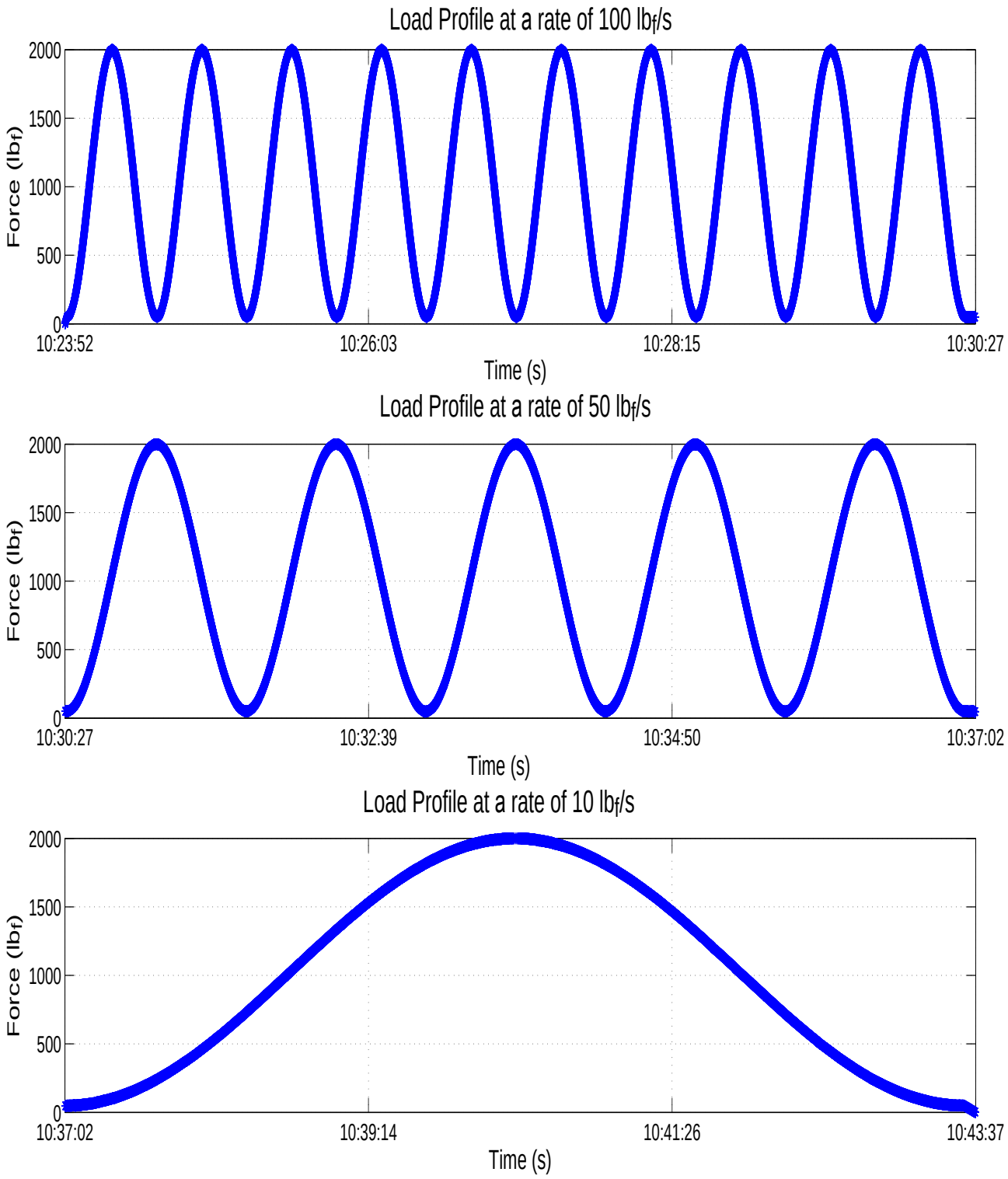

Figure 4.5: Varying Speed Profiles

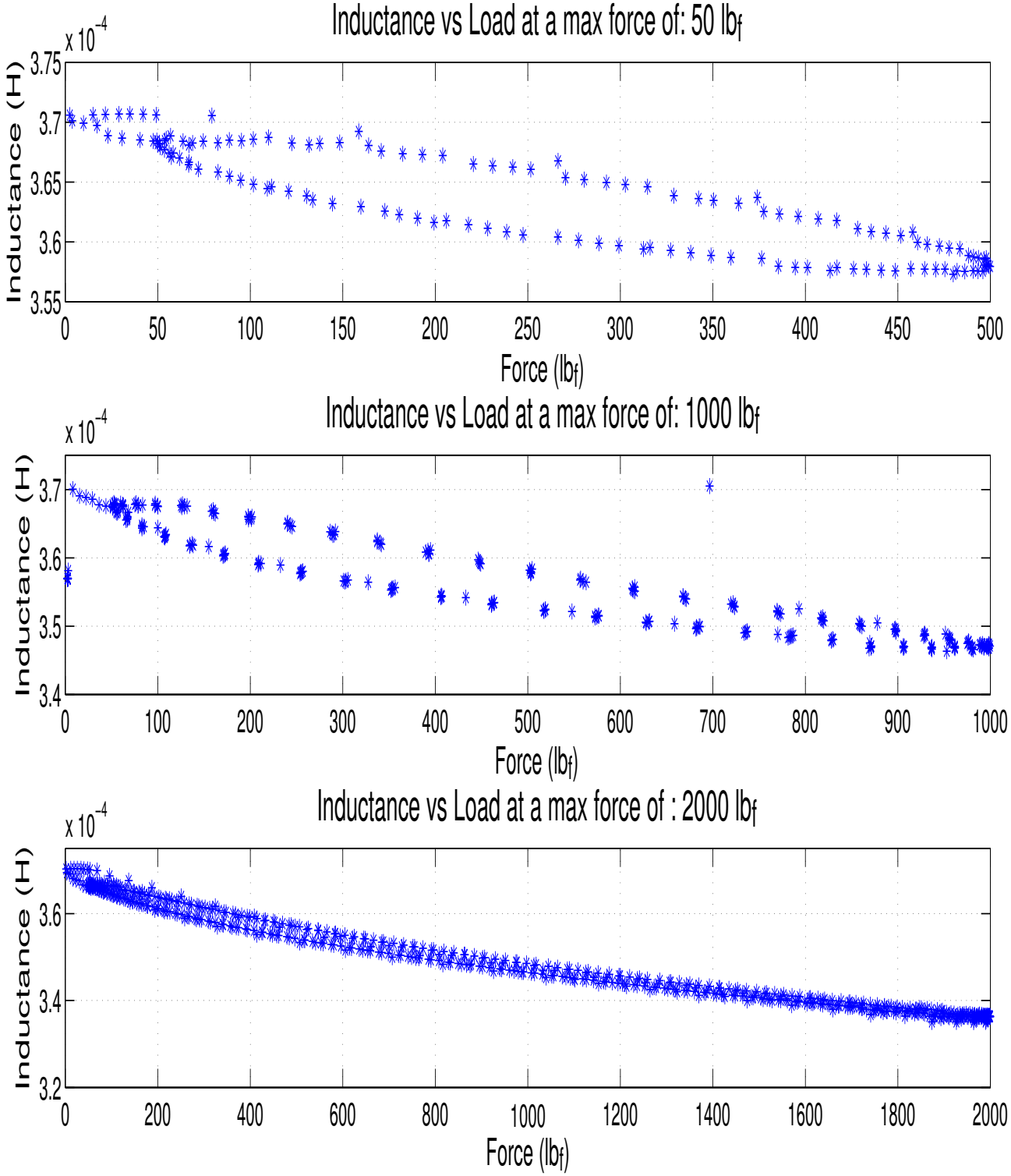

Figure 4.6: Varying Loads

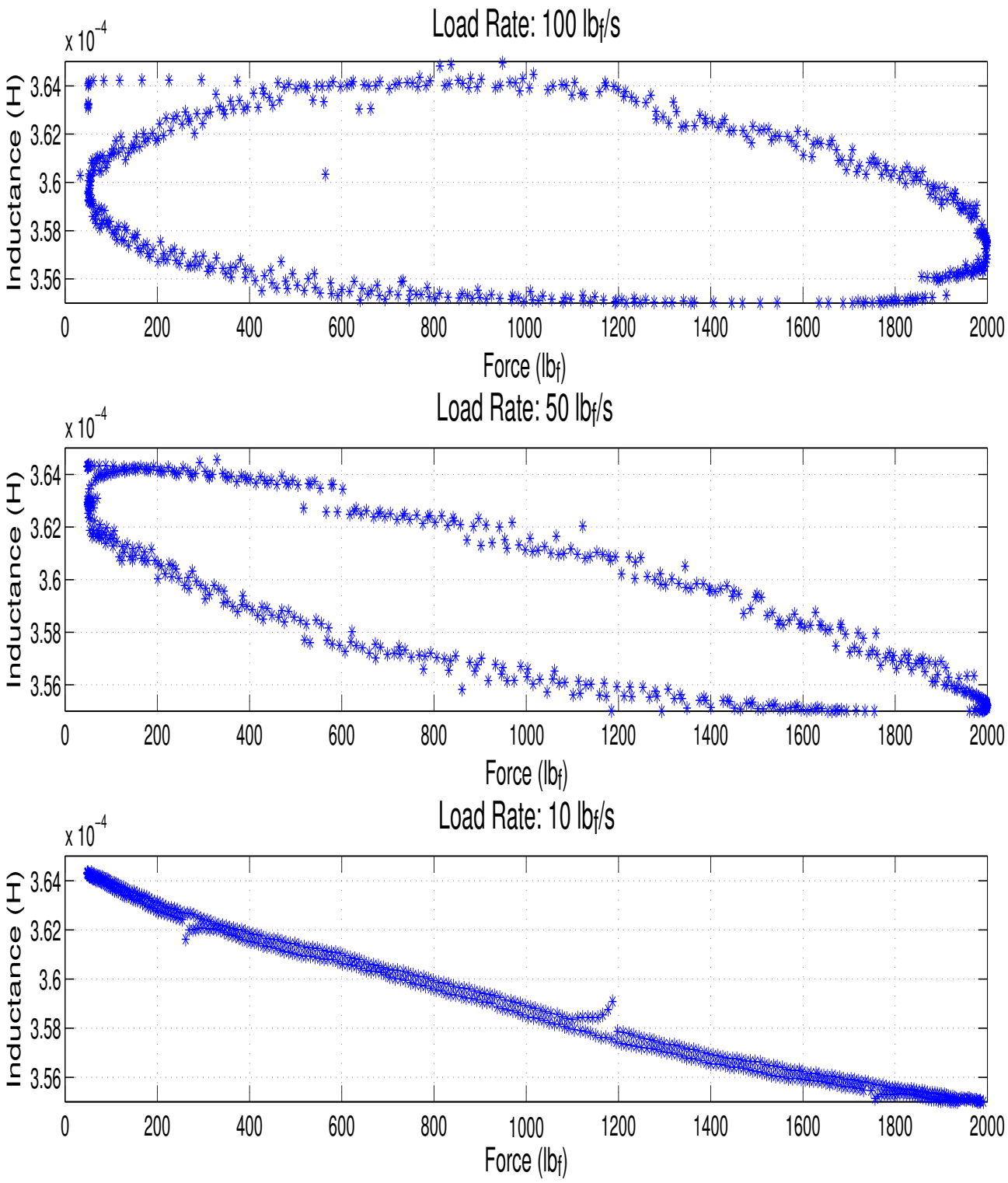

Figure 4.7: Varying Speeds

The results indicate that the effects of hysteresis decrease as the maximum load increases. However, this is merely an artifact of the lager ranges of inductance. The experiments with a larger load range have a higher overall fluctuation in inductance, causing the hysteresis to look smaller by comparison. Similarly, the reduction in hysteresis as the speed decreases may simply be an consequence of the way the meter reads inductance. To get an accurate reading, the meter collects multiple inductance readings over .3175 seconds and calculates the average. The latter suggests that fast changes in inductance will cause increased error when associating time stamps to the readings. To this end, a specialized load profile is created such that the load will be held constant long enough to get multiple accurate readings without masking the hysteretic effect. The load profile used for these trials is set to increment the load in 50 lb_f intervals, with a one second pause, and a loading rate change from 10.42 to 62.5 to 166.67 lb_f/s. The average of these rates together along with the one second pause equate to the previous rates of 10, 50, and 100 lb_f/s, respectively. The load profile is shown in Figure 4.8 and the response in Figure 4.9.

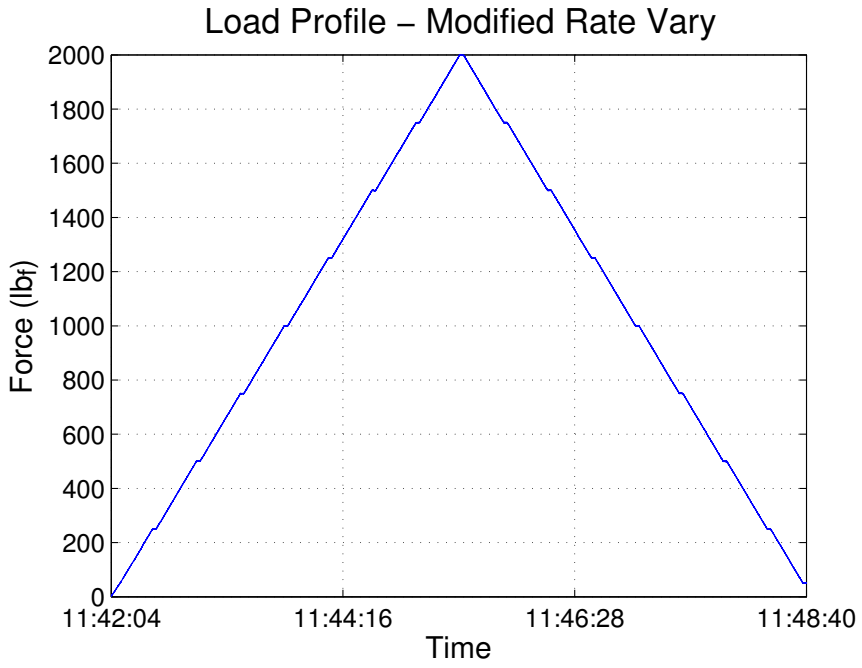

Figure 4.8: Modified Variable Rate Load Profile

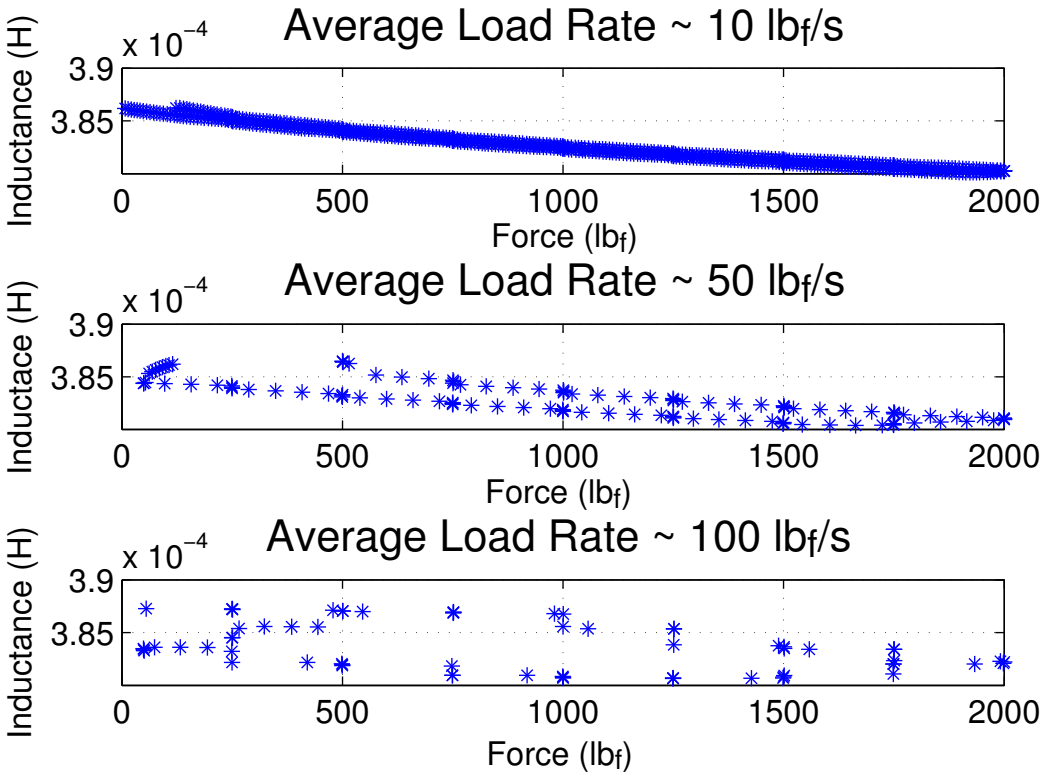

Figure 4.9: Modified Varying Rate Response

4.4 Trend Fitting

The results presented in Figure 4.9 prove that the load speed and not the data collection method is the cause for the hysteresis in the system. The latter necessitated additional testing to determine the exact relationship between the induction and load as well as to validate repeatability. Determining of the relationship is achieved by cycling the load at a rate of 10 lb_f/s for 10 cycles. Regression analysis is performed on the compiled data and a second order polynomial fit is implemented, where y is the Inductance (H) and x is the force (lb_f). The data with the fit can be seen in Figure 4.10 and the residuals in Figure 4.11.

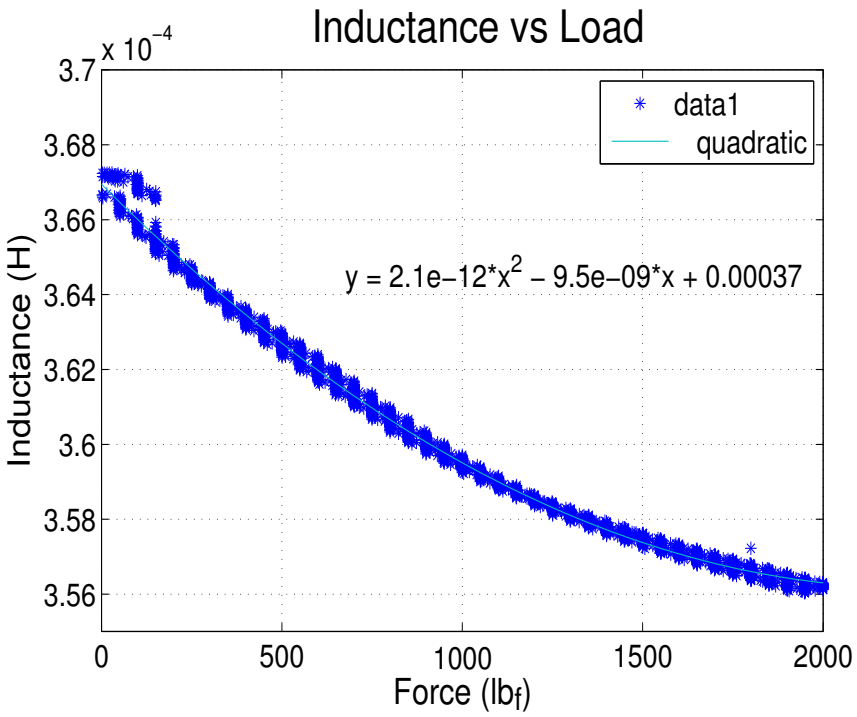

Figure 4.10: Final Load Fit

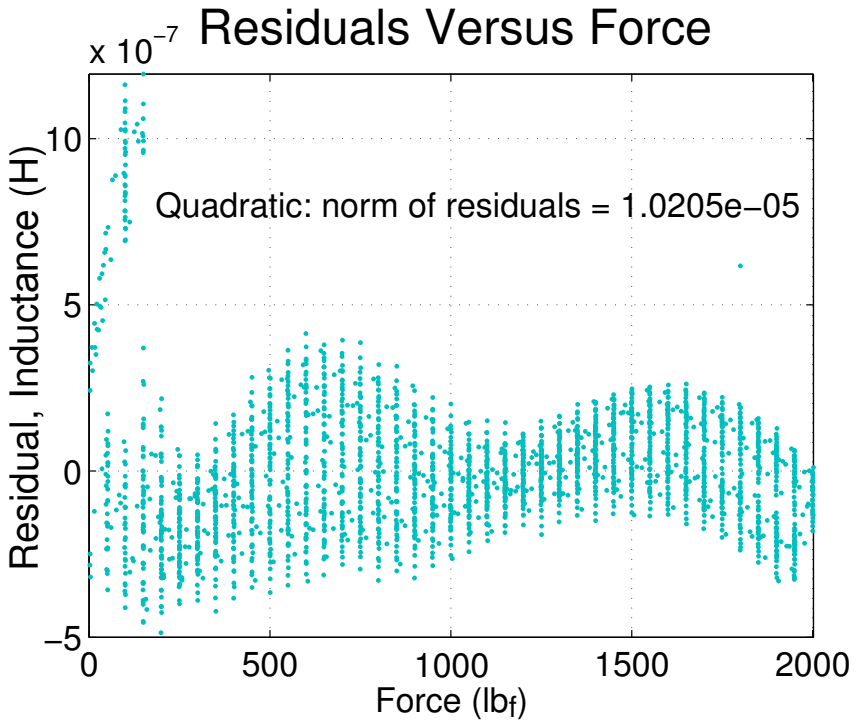

Figure 4.11: Final Load Fit Plot of Residuals

From the plot of residuals, the quality of the fit can be ascertained. In this case, the residuals have a range that is three orders of magnitude smaller than the range of values of the original data; thus showing the fit is adequate. To verify the efficacy of the quadratic fit on different data set, four more experiments are conducted and the same fit is applied to all collected data sets. The results of these experiments as well as the expected values are presented in Figure 4.12.

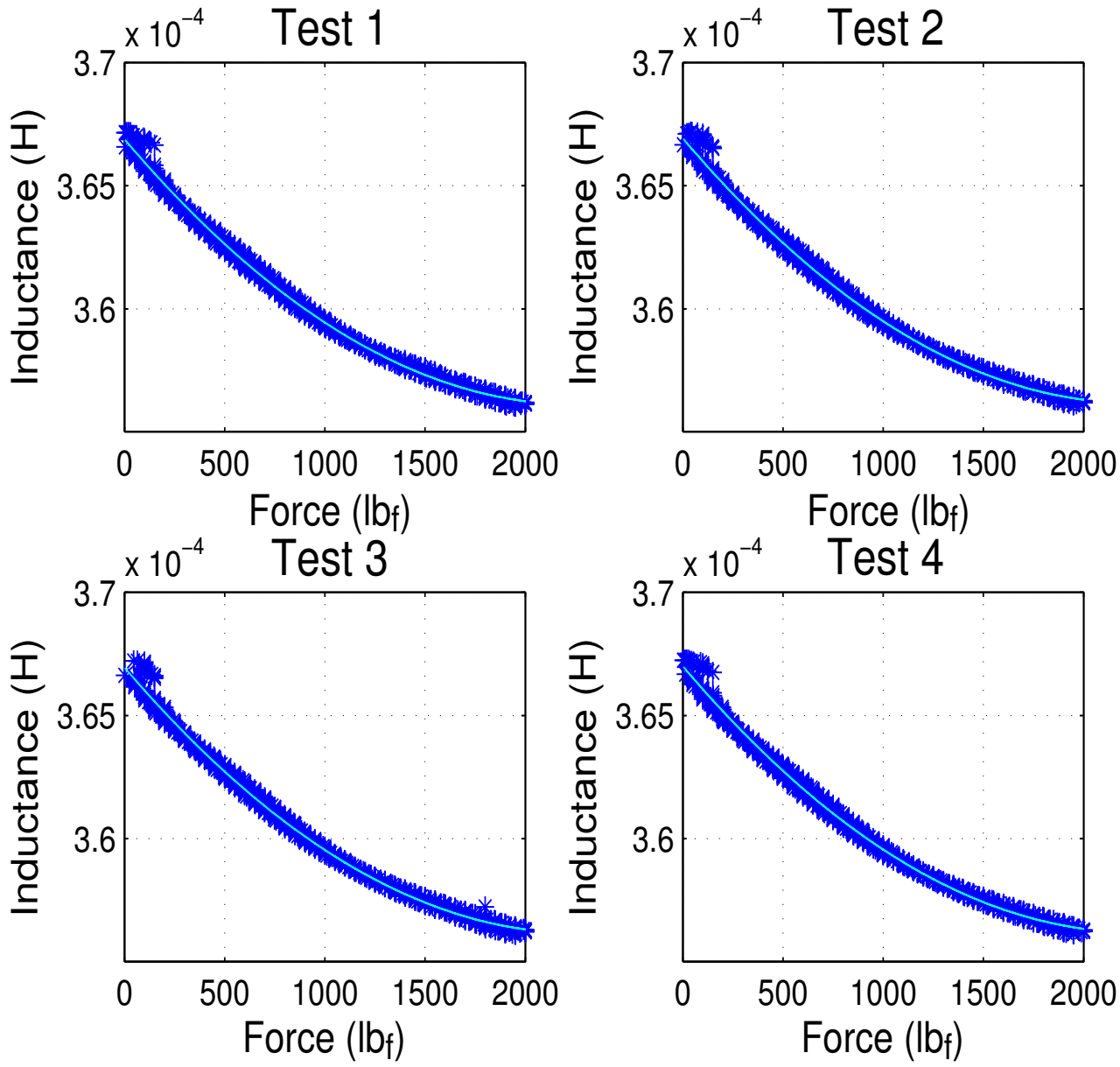

Figure 4.12: Quadratic Fit Test for Different Sets of Data

The experiments indicate that the sensor behaved in a predictable manner with an acceptable level of tolerance. Now that a relationship between the load and inductance has been properly established, it is necessary to approximate the relationship between inductance and relative magnetic permeability. By doing so, the behavior of any Terfenol-D based sensor can be characterized. The relationship between the inductance of a coil of wire and permeability can be approximated by:

$$L = \frac{\mu_0 \mu_r N^2 A}{l} \tag{4.5}$$

where L is the inductance, μ_0 is the magnetic constant ($4\pi \times 10^{-7} V \cdot s/(A \cdot m)$), μ_r is the relative permeability of the space inside the coil, N is the number of turns (200), A is the cross-sectional area (1.27 cm), and l is the length of the coil (1.07 cm). With a fixture design using the same size Terfenol-D rod, the inductance is approximately 16.76 times the relative permeability of the core. The error while using the fit in different data sets is within 10% in the regions of interest. It does, however, peak as high as 21.45% in a region where the MTS changes from loading to unloading. These results are displayed in Table 4.1.

Table 4.1: Load Error for Varying Data Sets

Force (lbf)	Calculated Force (lbf)	Percent Error (%)
3.979	36.87	8.3
599.9	561.1	6.5
1200.0	1290.0	7.5
1801.0	1831.0	1.7
1600.0	1595.0	0.3
1000.0	1054.0	5.4
399.0	384.5	3.6
249.7	251.1	0.6
848.9	820.6	3.3
1449.0	1498.0	3.4
1950.0	1848.0	5.2
1350.0	1398.0	3.6
750.1	778.1	3.7
150.5	178.2	18.4
500.1	424.2	15.2
1100.0	1117.0	1.6
1700.0	1703.0	0.2
1701.0	1668.0	1.9
1119.0	1169.0	4.4
536.0	497.0	7.3
150.6	182.8	21.5
750.1	690.2	8.0
1350.0	1393.0	3.1
1949.0	1905.0	2.3
1449.0	1460.0	0.7
849.0	875.3	3.1
250.2	252.5	0.9

CHAPTER V.

ENERGY HARVESTING & INTEGRATION

The conversion of mechanical stress to an electric potential was first discovered in 1881 when Gabriel Lippmann mathematically deduced the converse effect of pyroelectricity. Piezo-electric materials are similar in nature to pyroelectric materials, creating electricity from mechanical stress as opposed to heat. They are often chosen due to their ease of use, creating a potential difference at opposing ends of their crystal structure under applied pressure. However, piezoelectric materials do not generally yield high power generation, normally producing 1 to 2 mW under nominal conditions. Conversely, magnetostrictive materials are able to generate more power, albeit at a lower voltage. Many applications for low power are optimized using low voltage circuitry. Another limiting factor for piezoelectrics in applications with a harsh environment is their ceramic nature, making them have a short operable lifespan. Magnetostrictive materials are much more durable when properly oriented and protected. A fixture can be designed to allow a magnetostrictive alloy to withstand harsher environments. Terfenol-D is chosen for this application due to it having the largest magnetostriction of any alloy. In order to adapt the previous fixture (Modified Magnetic Field Insulating Fixture) to generate power, magnets are placed on either end of the Terfenol-D rod. These magnets generate a magnetic field across the Terfenol-D core. When the fixture is either compressed or stretched, the relative permeability of the core changes. This change in permeability causes a fluctuation in the magnetic field emanating from the magnets, thereby generating a current in the coils of wire. That current can then be harvested using numerous methods and stored for future use. The induced voltage in a coil can be estimated by using the formula:

$$V_{induced} = (d\phi)/(dt) \tag{5.1}$$

$$= NA(dB/dt) \tag{5.2}$$

where ϕ is the magnetic flux present inside the Terfenol-D core, t is time, N is the number of turns, A is the cross-sectional area of the coil, and B is the strength of the magnetic field.

5.1 Initial Energy Harvesting

Initial energy harvesting experiments were conducted using the largest magnets available ($4500 Gauss$) with the understanding that the stronger the magnetic field, the greater the flux will be for a set change in permeability. The experiment is conducted using a 300 turn coil with a base inductance of $350 \mu H$(microHenry) inside of the "Modified Magnetic Field Insulating Fixture". The rate of load is increased from $16 kips$ to $120 kips$. Results for the initial energy harvesting experiments are shown in Figure 5.1.

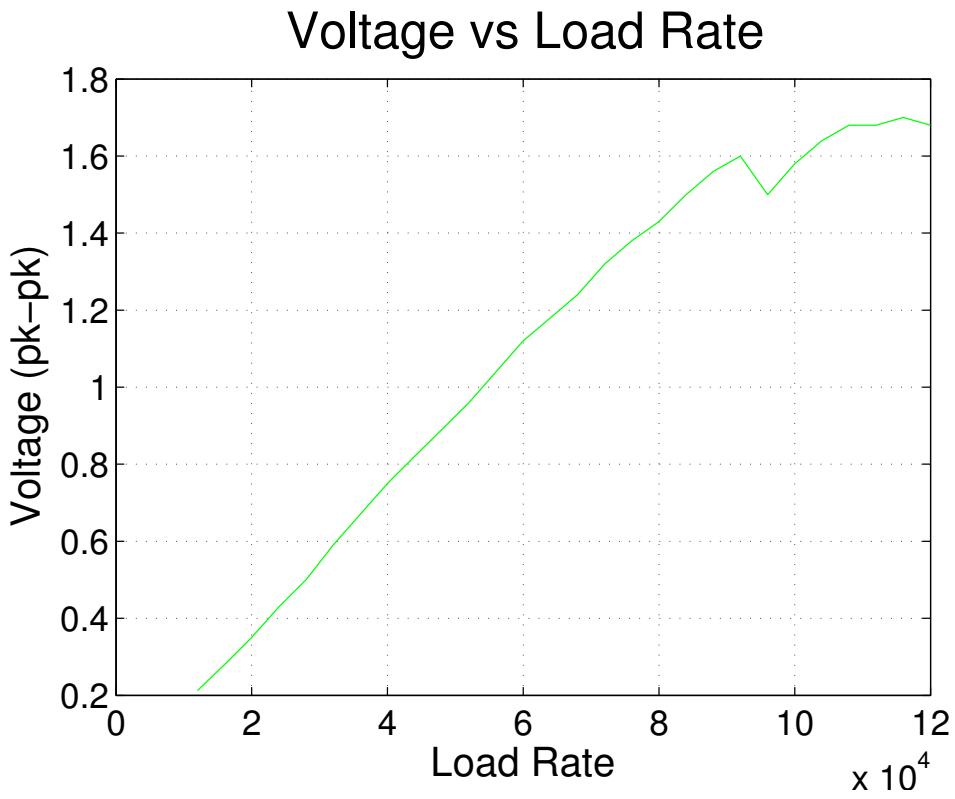

Figure 5.1: Initial Energy Harvesting Experiment

The relationship between the rate of changing load and the voltage generated has an almost linear relationship up until 88 lb_f/s, meaning that either the limitations of the MTS were reached, or 1.7 V_{pk-pk} is the maximum voltage these conditions can produce. Nevertheless, the power generated between 80 and 120 kip/s is more than sufficient to power a wireless bearing health monitoring system. With a general trend in mind, the experiment is repeated three more times to validate accuracy and repeatability. The recorded measurements are listed in Table 5.1 for simpler comparison across the three trials.

Table 5.1: Voltage Generation vs Load Rate Change

Rate (lb_f/s)	$V_{pk-pk}Test1$	$V_{pk-pk}Test2$	$V_{pk-pk}Test3$
20000	0.35	0.35	0.35
24000	0.44	0.43	0.43
28000	0.51	0.5	0.5
32000	0.59	0.58	0.59
36000	0.67	0.66	0.67
40000	0.75	0.75	0.75
44000	0.82	0.82	0.82
48000	0.9	0.89	0.89
52000	0.96	0.96	0.96
56000	1.04	1.04	1.04
60000	1.12	1.12	1.12
64000	1.18	1.19	1.18
68000	1.25	1.24	1.24
72000	1.32	1.32	1.32
76000	1.4	1.38	1.38
80000	1.44	1.43	1.43
84000	1.52	1.52	1.5
88000	1.54	1.54	1.56
92000	1.6	1.62	1.6
96000	1.54	1.52	1.5
100000	1.6	1.58	1.58
104000	1.66	1.64	1.66
108000	1.7	1.7	1.68
112000	1.7	1.7	1.68
116000	1.7	1.7	1.7
120000	1.7	1.7	1.68

The power can be calculated from the voltage measured with a known impedance for the coil. The impedance over a range of frequencies can be obtained for a coil by using the formula for the impedance of a coil at a given frequency and deriving the real resistance of the wire. The meter used for the duration of these experiments can measure the inductance at several testing frequencies: 100 Hz, 120 Hz, 1 kHz, and 10 kHz . Those values, in conjunction with the series resistance present in the wire, can then be used to determine the exact impedance of the coil necessary for determining the generated power:

$$Z = R_1 + R_2 \tag{5.3}$$

$$R_1 = \rho l/A \tag{5.4}$$

$$R_2 = j\omega L \tag{5.5}$$

$$\omega = 2\pi f \tag{5.6}$$

Where Z is the total impedance of the coil, $R1$ is the real part of the impedance, $R2$ is the imaginary impedance, l is the length of the wire, A is the cross-sectional area, ρ is the resistivity of the copper, j is the square root of −1, L is the inductance of the coil, and f is the frequency of the system. It is difficult to measure the exact length of wire used to hand wind an inductor, however, the real impedance can be approximated by using the LCR meter and subtracting the imaginary impedance of the inductor. The inductance and impedance are measured at 100 Hz because it is the closest to the frequency range that will be used

$$R_1 = Z - R_2 \tag{5.7}$$

$$R_1 = (2.62 + j0.8466) - (j(2\pi(100Hz))(1.3483mH) \tag{5.8}$$

$$R_1 = 2.62 + j0.85 - j0.85 \tag{5.9}$$

$$R_1 = 2.62\Omega \tag{5.10}$$

Ideally, the voltage induced in a coil can be mathematically approximated using the formula:

$$P_{available} = V_{rms}^2/(4Re(Z)) \tag{5.11}$$

$$= (1.8v)^2/(4(2.62\Omega + j(2\pi(30Hz))1.3483mH)\Omega) \tag{5.12}$$

$$= (3.24v^2)/(4 * 2.63\Omega) \tag{5.13}$$

$$\approx 31mW \tag{5.14}$$

5.2 Ranging Magnetization

While the power generated from the initial energy harvesting experiments is sufficient to power a low-power on-board monitoring system during ideal conditions, it is still necessary to determine how the power generated is related to the level of magnetization and if anything else can be done to maximize power generation. Doing so would ensure that enough power is harvested even under unfavorable conditions. For this reason, five magnets of varying strengths from 2450 to 6150 Gauss are selected for testing. The same experiment is repeated several times for each magnet and then the average is taken across the trials. The acquired results are shown in Figure 5.2

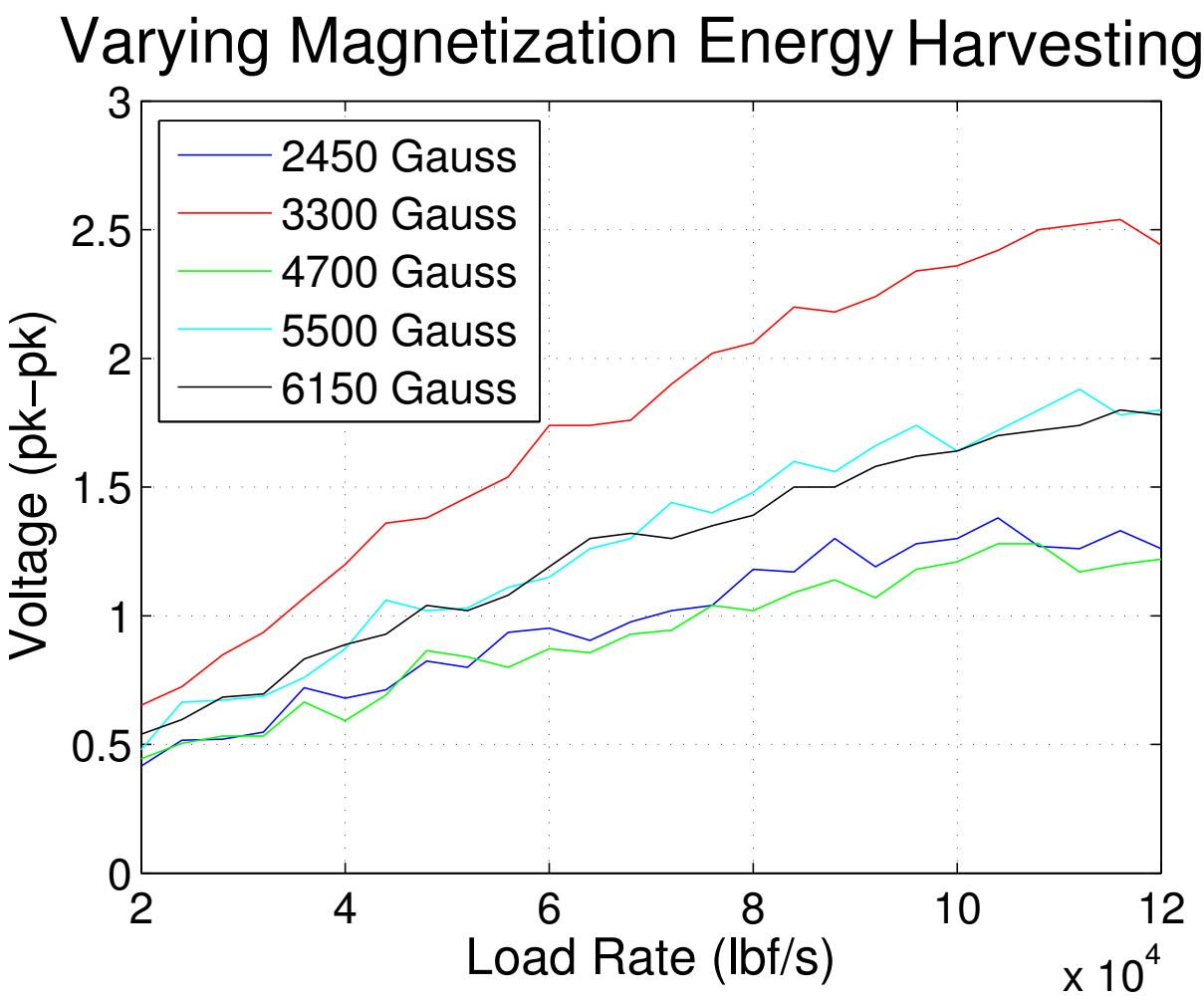

Figure 5.2: Varying Magnetization Energy Harvesting

5.3 Maximum Available Power

From the plot shown in Figure 5.2, it can be noted that more energy was generated in a particular range of magnetization. This can be attributed to the magnetostrictive properties of Terfenol-D saturating below and above certain levels of magnetization. The relationship between the magnetosrictive strain and the applied field under different loads is shown in Figure 5.3.

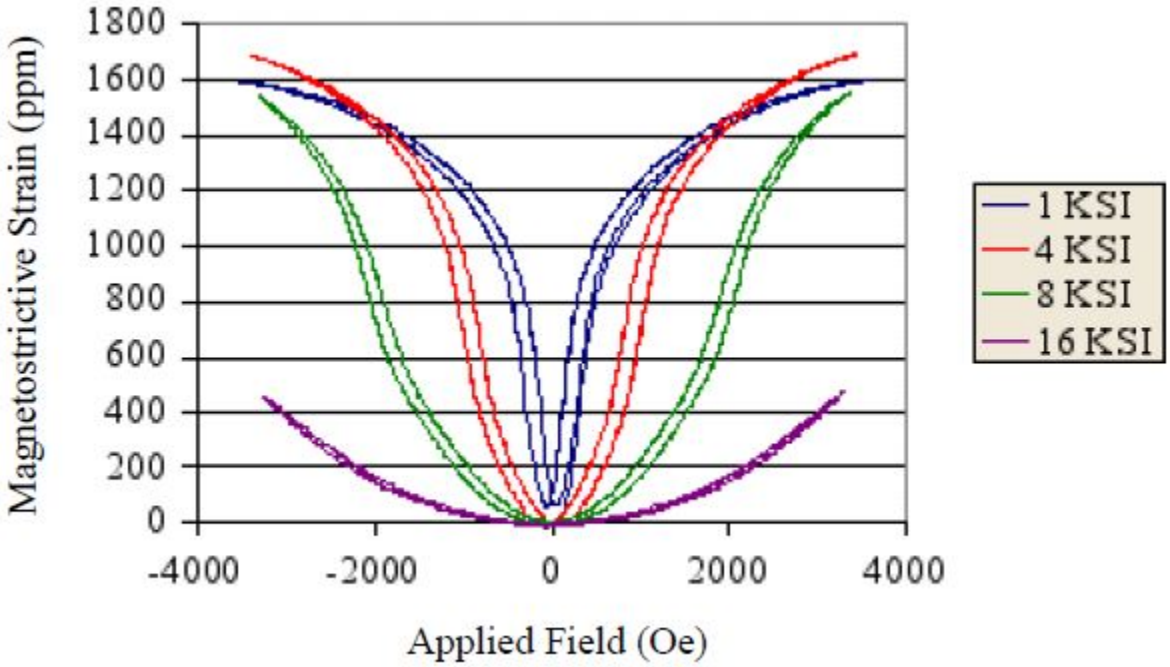

Figure 5.3: Terfenol-D Versus Field at Various Preloads [1]

From the trends observed in Figure 5.3, a relationship for the applicable load range can be interpolated. The power generated by the fixture is dependent on the amount of flux created in the magnetic field. The flux in turn is directly related to the magnetostrictive strain of the Terfenol-D. Therefore, maximum power generation can be achieved during the linear segment of the curve. The only magnets available that are within this region are those with 3300 Gauss of magnetic flux density. Further experiments are conducted using those magnets to characterize the power generation and verify repeatability and reliability. The results of these tests along with an appropriate correlation are provided in Figure 5.4.

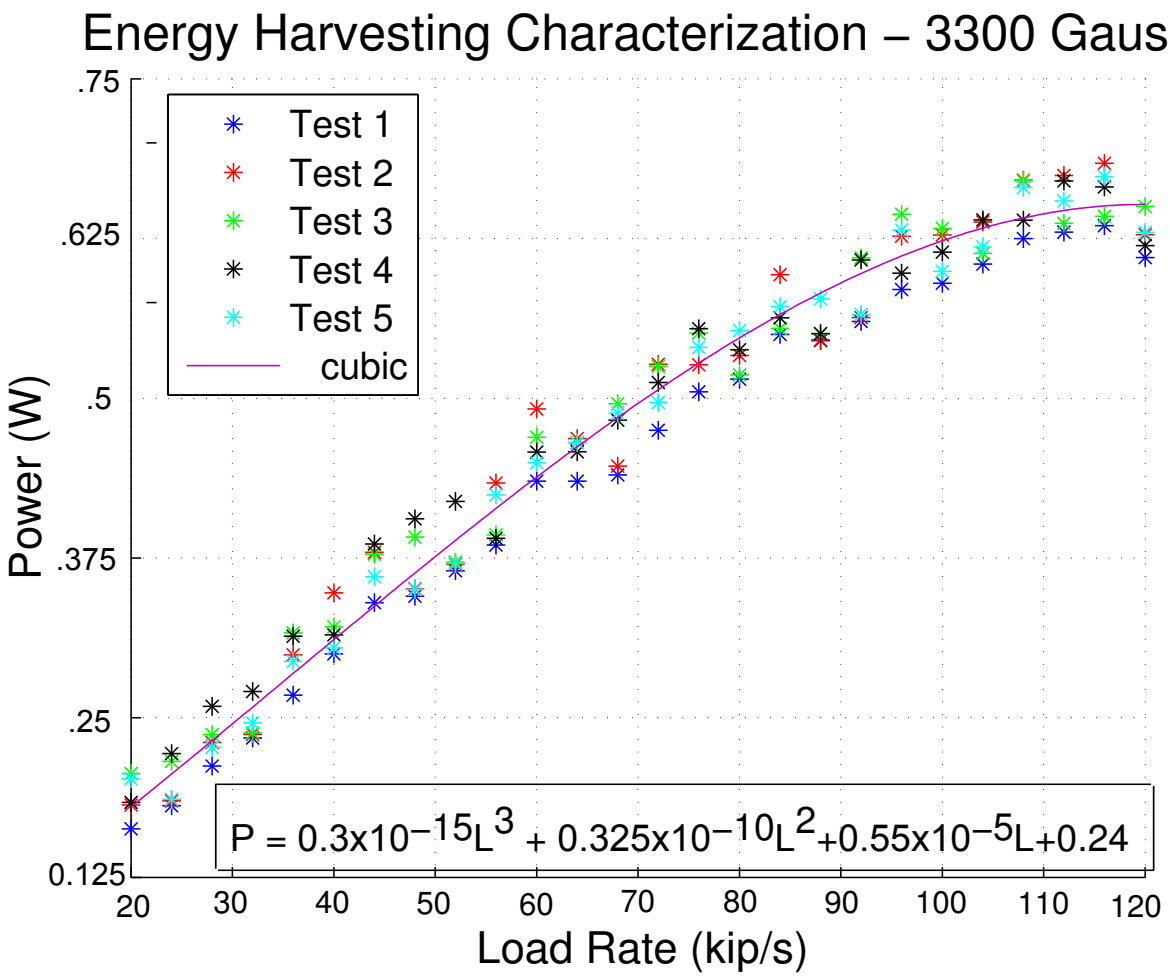

Figure 5.4: Optimal Energy Harvesting Characterization

The tests performed at nominal magnetization, indicate that a maximum power of 0.67 W is feasible with a sustainable power generation of 83 mW. If the aforementioned conditions are available for at least ten seconds, enough energy will have been generated to power a 40 mW on-board monitoring system for at least twenty seconds. That amount of time is sufficient for relevant data to be recorded and transmitted. Therefore, an average of ten seconds of optimal excitation conditions (i.e. 120 kip/s of compression) available every four minutes would be sufficient to power such systems.

5.4 Integration

The sensor designed using a Terfenol-D core is considerably larger than the load cells currently used, as well as far more expensive to implement. For the sensor to be considered feasible, it must also be able to generate energy in the same configuration. To determine the best possible scenario for both energy harvesting and static load sensing, a variety of tests similar to those used in the load sensing characterization are conducted using each pair of magnets. As can be seen in Figure 5.2, useful energy can be generated across various levels of magnetization. The load profile used for this experiment varies the rate of load from 100 to 50 lb_f/s to 10 lb_f/s and is shown in Figure 5.5. The results are separated into three different groups for the various load rates, they are displayed in Figure 5.6, Figure 5.7, and Figure 5.8.

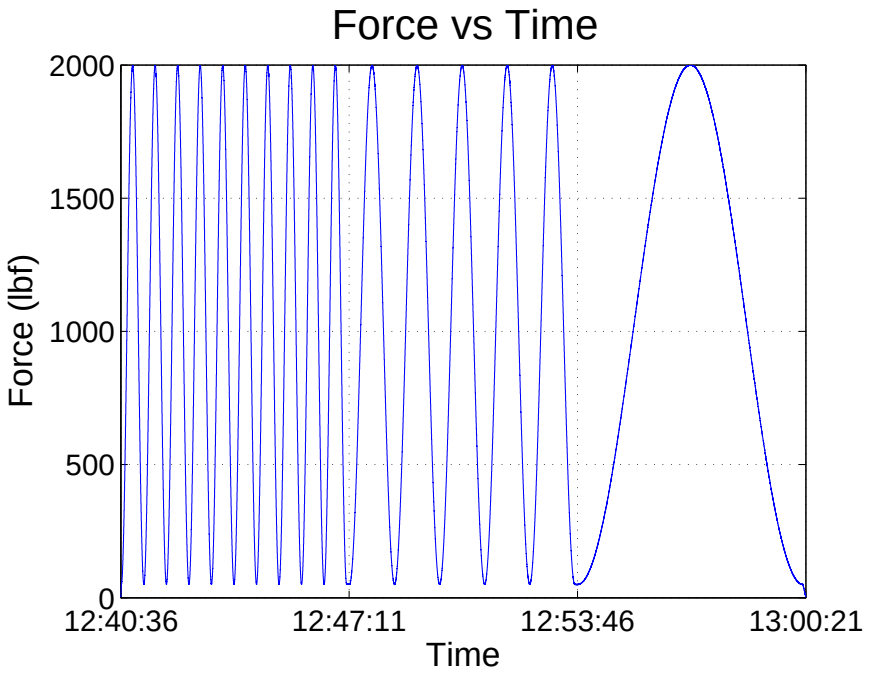

Figure 5.5: Integration Load profile

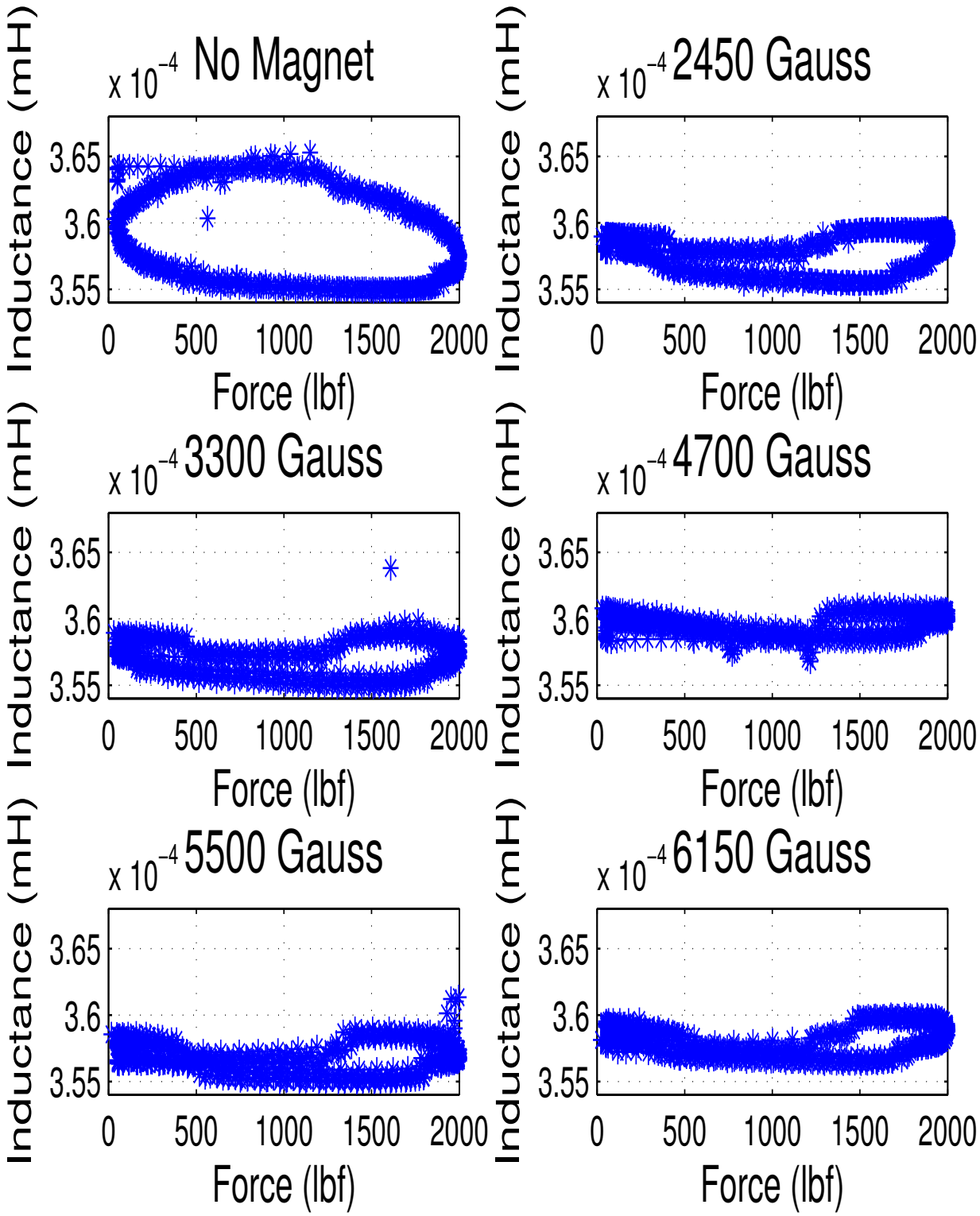

Figure 5.6: Inductance vs Load with Magnetization - 100 lb_f/s

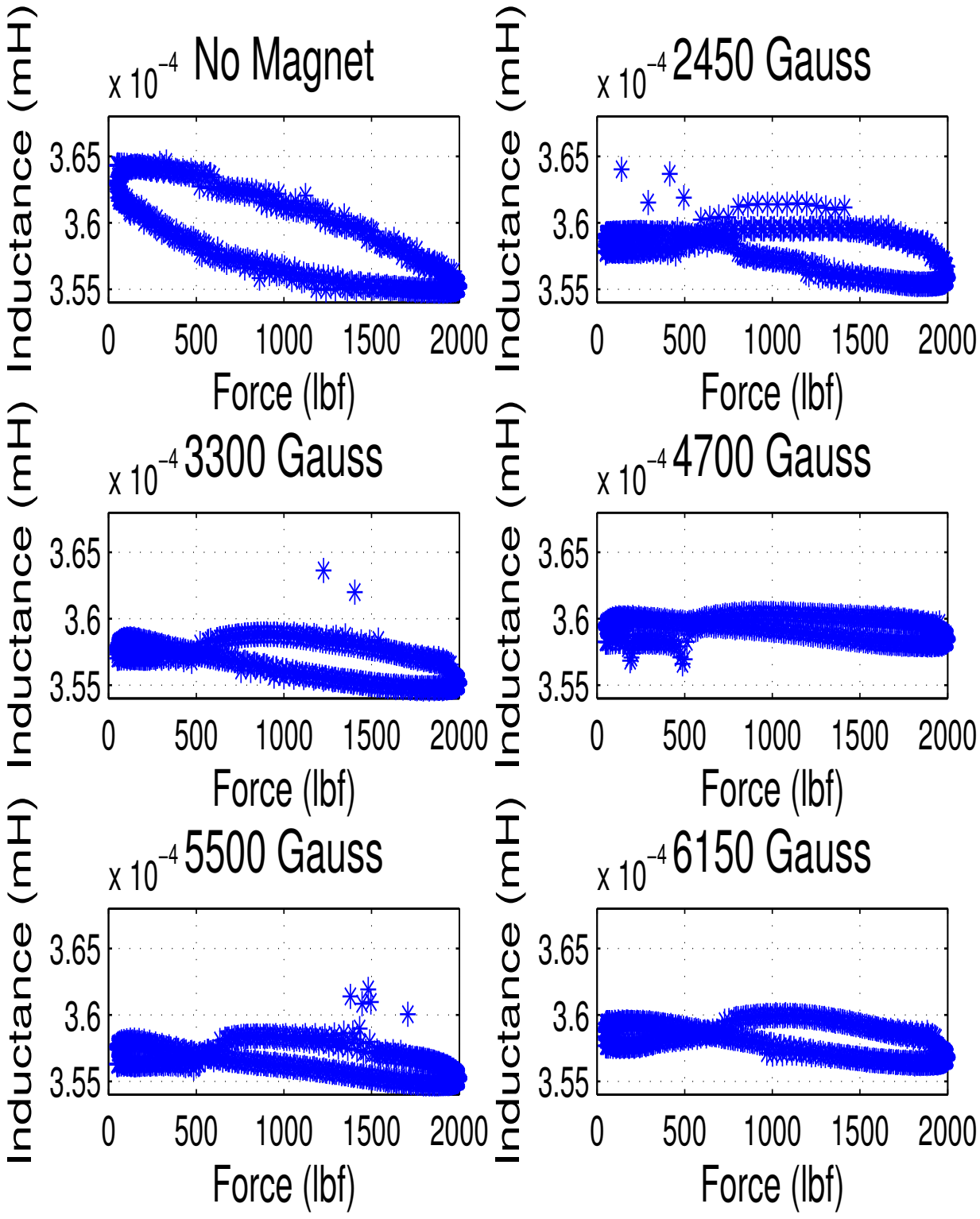

Figure 5.7: Inductance vs Load with Magnetization - 50 lb_f/s

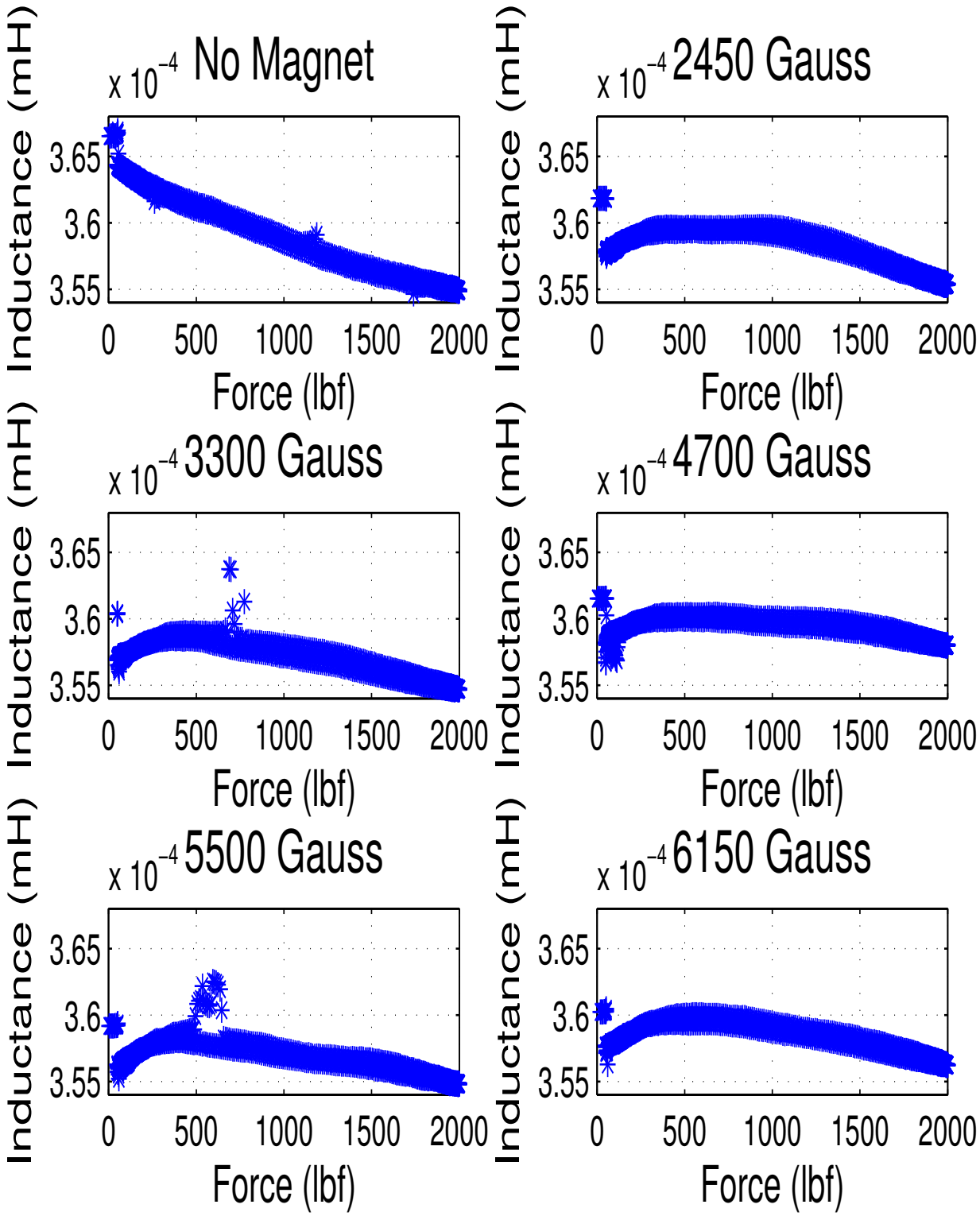

Figure 5.8: Inductance vs Load with Magnetization - 10 lb_f/s

Upon observation, it is clear that once again the lower the load rate, the more predictable the response. Interestingly enough, any magnetization on the material changes the nature of the relationship between the force applied and the inductance measured. Unfortunately, this new behavior is not favorable for a sensor. With repeated x values for a given y value, it is impossible to determine which of the x values is the current one. In most of these cases, the inductances are exclusive to a force above 1500 lb_f. Fixtures can be designed around this limitation making these levels of magnetization workable for railroad bearing health monitoring. However, the purpose of this section is to determine the compatibility of the energy harvesting together with the load sensing aspects. With a fixture that limits the load between 1500 and 2000 lb_f there would not be enough magnetic flux to generate the energy necessary for operation.

CHAPTER VI.

CONCLUSION AND FUTURE WORKS

The experiments conducted in this project consisted of several applications for magnetostrictive materials in the real-time monitoring of vehicle suspension components. Long term monitoring of which, can be improved through the use of wireless, self-powered sensors. The necessity for the applications discovered was made evident by the railroad bearing health monitoring studies conducted at UTPA. These applications consisted of energy harvesting and load detection. Terfenol-D was chosen for these studies due to its giant magnetostriction and mechanical properties.

6.1 Material Characterization

Throughout the characterization of the material several properties were measured: hardness, relative permeability at no load, and Young's modulus. The software necessary for the operation of the Material Test System (MTS) was programmed with several different test patterns and load profiles for a variety of situations. In a similar fashion, a Matlab script was developed to interface with the LCR meter and properly record measurements. Hardness was determined through the use of Vicker's hardness test in accordance with ASTM E92 [9], resulting in a value of 63.5. Young's Modulus was measured using the MTS, compressing the material and determining the ratio of stress to strain during the region of elasticity. The material did not yield under the maximum pressure exerted by the MTS, however, Young's Modulus (22 GPa) was still extractable from the data collected. Lastly, the relative permeability at no load is measured by creating an inductor with Terfenol-D at its core and measuring the inductance. From said inductance, the relative permeability was derived (3.705).

6.2 Fixture Design

Many iterations of the fixtures were fabricated throughout the duration of the experiment, each providing more functionality than the last. Initially, the fixture was a simple "washer-spool" model. This model consisted of the readily available washers affixed to either end of the Terfenol-D core using 5-minute epoxy, which was then wound with magnet wire. The configuration initially had significant hysteresis and did not provide sufficient protection to the core of the sensor. After continuing testing, it was determined that the platens used by the MTS were not perfectly parallel, causing the fixture to move during testing, leading to inconsistent results. To remedy this, an auto-leveling platen, shown in Figure 3.7, was used. Creation of the magnetic model of the initial fixture proved to be difficult due to the unknown alloy used for the washers. A new "Stainless Steel Spool Fixture" was created using washers made of 316 Stainless steel affixed around the core rather than the ends. This new arrangement allowed the entirety of the force to be applied to the Terfenol-D. Unfortunately, the Terfenol-D core was still exposed and damaged, while the magnetic field flowing through the outside of the fixture caused the sensor to behave differently on different surfaces. For these reasons, a fixture was designed that not only limited the force to one axis, but also directed the majority of the magnetic field through the core of the fixture. This "Magnetic Field Insulating Fixture" kept the Terfenol-D cores from being damaged during normal operation, all the while confining the majority of the magnetic field. A taller version of this fixture was created soon after to accommodate the extra height necessary for power generation.

6.3 Load Sensor Characterization

A very important factor in determining the health of a bearing is the amount of load present. To properly characterize the sensor created, it is first necessary to determine the range of loads which the sensor must be able to detect. This is achieved by analyzing the pressure film study, shown in Figure 4.2 and determining the force for the cross sectional area of the sensor. After which, initial load experiments were conducted to ascertain the general nature of the relationship between load and inductance. The results generated indicate a negative trend. Further testing is conducted to

determine the effect the load range and load rate have on said relationship. The tests confirm that while the material is in the elastic region, the load range has no effect on the relationship. The load rate on the other hand, greatly impacts the nature of the relationship, making the sensor most viable as a static load sensor. Once the parameters and environment of the sensor were adequately accounted for, it was then time to properly characterize the relationship and determine the quality of the fit.

6.4 Energy Harvesting and Integration

The generation of electricity from excitation is a novel concept, which, can greatly improve real time on-board health monitoring systems. Initial experiments showed more than sufficient energy could be generated in the lab using readily available materials. Subsequent experiments proved that useful amount of power is available across varying levels of magnetization. Preliminary calculations estimated that the designed energy harvester is capable of generating a sustainable power generation in the range of $30-60\ mW$. The actual power generated was more than $80\ mW$. Moreover, this power range is significantly higher than the $1-2\ mW$ of power generated by existing Terfenol-D devices. With the advancements made in low power electrical component design, the power generation levels produced by the developed Terfenol-D energy harvester are sufficient to run low-power bearing health monitoring systems. An example of the power consumption of the main components required for a bearing health monitoring system is shown in Table 6.1. Before claiming that the sensor can be used to detect load and generate energy, it is first necessary to determine whether these functions can be used in the same configuration. This is done by conducting load profile experiments, similar to those from Chapter IV. Consequently, it was verified that the energy harvesting and load detection functions of the sensor have different optimal operating conditions.

Table 6.1: Power Consumption of Main Components

Component	**Power Consumption (mW)**
Microcontroller	5
Accelerometer	1
Strain gauge	1
Thermocouple	1
Transmitter	20
Assorted Supporting Circuitry	5
Total	**33**

6.5 Future Work

There is much work that must still be done in the applications proved in this project, as well as those yet to be proven. Regarding the load sensing aspect, an oscillator/PIC circuit can be designed to simplify the load detection from measuring inductance to voltage. This will reduce the equipment necessary for operation (LCR meter, computer running Matlab) and can even be outfitted with an LCD to display current load. Energy harvesting applications can also be improved by designing a charging circuit to optimize the harvesting and regulate the voltage to usable levels. There are still applications that have yet to be fully investigated, such as vibration detection. Although the sensor designed would probably differ greatly from current designs, it would still be prudent to investigate vibration detection as it is a very important indicator for bearing health.

REFERENCES

[1] Etrema Products. Data sheet: Terfenol-d, 2012. Online: http://www.etrema-usa.com/documents/Terfenol.pdf.

[2] Sean Woods. Development of algorithms and criteria for continuous condition monitoring of railroad bearings, 2012.

[3] Ji Li Liang Yin Sixing Yi, Erqing Zhang and Shufanf Li. Throughput Optimization for Self-Powered Wireless Communications with Variable Energy Harvesting Rate. Technical report, Testing Center of The State Radio Monitoring Center, Beijing, China, 2013.

[4] Pangang LIU Xinshen LI Ping LI, Yumei WEN and Chaobo JIA. An Electromagnetic Energy Harvesting Circuits for Self-Powered Wireless Sensor Network. Technical report, The Key Laboratory for Optoelectronic Technology & Systems, Ministry of Education, 2008.

[5] Xianzhi Dai Zhang Zhang and Yong Wang. An Improved Magnetoelectric Vibration Energy Harvester for Wireless Sensors. Technical report, School of Physics and Electronic Information, China West Normal University, 2012.

[6] Zagar Bernhard G. Oppermann Klaus. A Novel Magneto-Elastic Force Sensor design Based On Terfenol-D. Technical report, Institute for Measurement Technology, Johannes Kepler University Linz, 2009.

[7] R. D. Greenough K. Prajapti and A. Wharton. Effect of Cyclic Stress on Terfenol-D, institution = Department of Applied Physics, University of Hull, type = Technical Report, year = 1996,. Technical report.

[8] Supratik Datta and Alison B. Flatau. Quasi-Static Characterization and Modeling of the Bending Behavior of Single Crystal Galfenol for Magnetostrictive Sensors and Actuators. Dissertation, 2009.

[9] ASTM E92-82(2003), Standard Test Method for Vickers Hardness of Metallic Materials, ASTM International, West Conshohocken, PA, 2003, www.astm.org. Technical report.

APPENDIX A

SOLIDWORKS MODELS

Figure 0.1: .75" Terfenol-D rod

Figure 0.2: 2450 Gauss Magnet

Figure 0.3: 3300 Gauss Magnet

Figure 0.4: 4700 Gauss Magnet

Figure 0.5: 5500 Gauss Magnet

Figure 0.6: 6150 Gauss Magnet

Figure 0.7: MFI Short Base

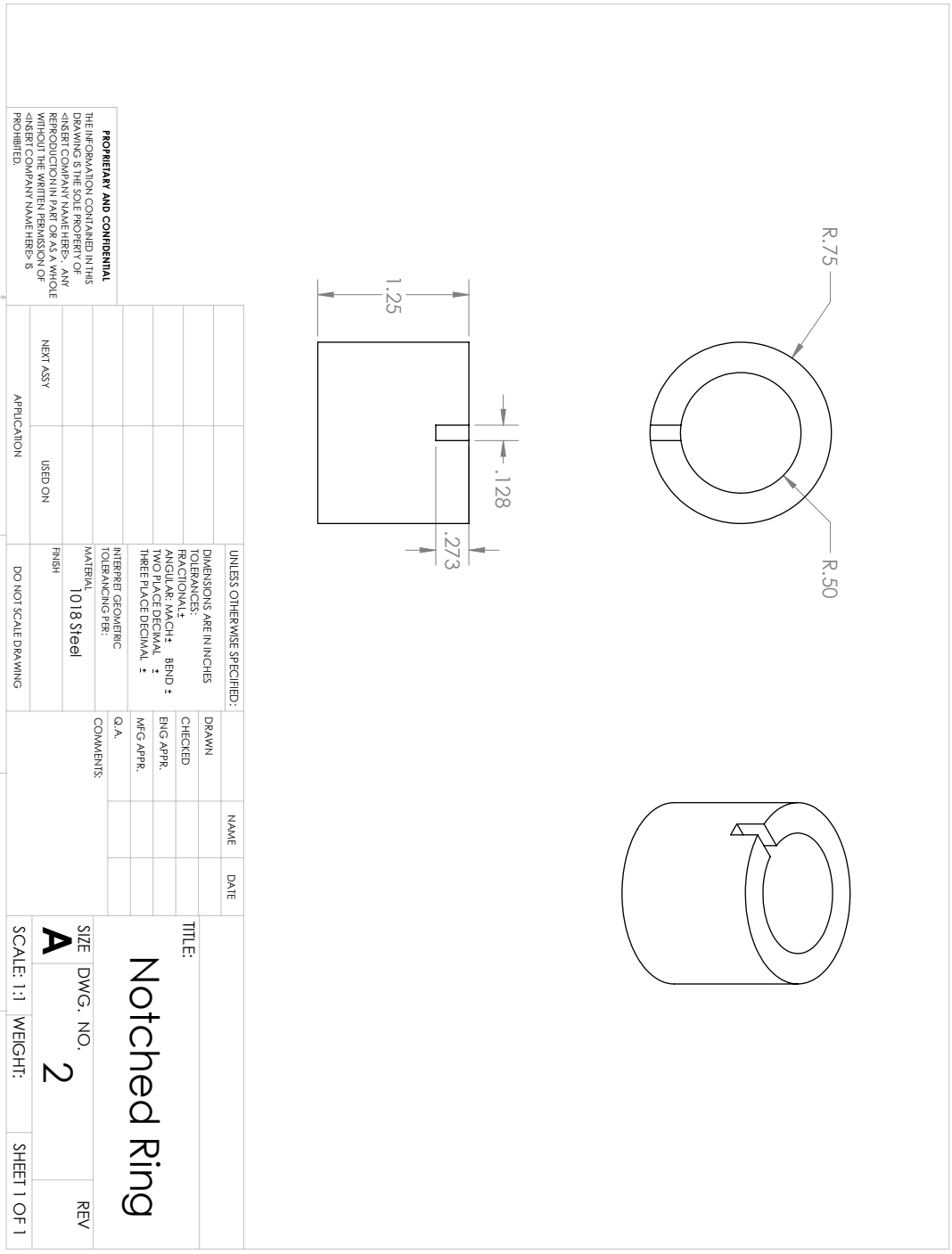

Figure 0.8: MFI Short Ring

Figure 0.9: MFI Short Rod

ITEM NO.	PART NAME	DESCRIPTION	QTY.
1	Rod	1018 Steel	1
2	Notched Ring	1018 Steel	1
3	Terfenol	$Tb_3Dy_7Fe_2$	1
4	Spool	Aluminum	1
5	Coil	Magnet Wire: size 26 AWG, 200 turns	1
6	Washer-.075"	Aluminum	1
7	Base	1018 Steel	1

UNLESS OTHERWISE SPECIFIED:
DIMENSIONS ARE IN INCHES
TOLERANCES:
FRACTIONAL ±
ANGULAR: MACH ± BEND ±
TWO PLACE DECIMAL ±
THREE PLACE DECIMAL ±
INTERPRET GEOMETRIC TOLERANCING PER:
MATERIAL
FINISH
NEXT ASSY
USED ON
APPLICATION
DO NOT SCALE DRAWING

NAME | DATE
DRAWN
CHECKED
ENG APPR.
MFG APPR.
Q.A.
COMMENTS:

TITLE:
Magnetic Field Insulating Fixture Short Assembly

SIZE A | DWG. NO. | REV
SCALE: 1:1 | WEIGHT: | SHEET 1 OF 1

Figure 0.10: MFI Short Assembly

Figure 0.11: MFI Tall Base

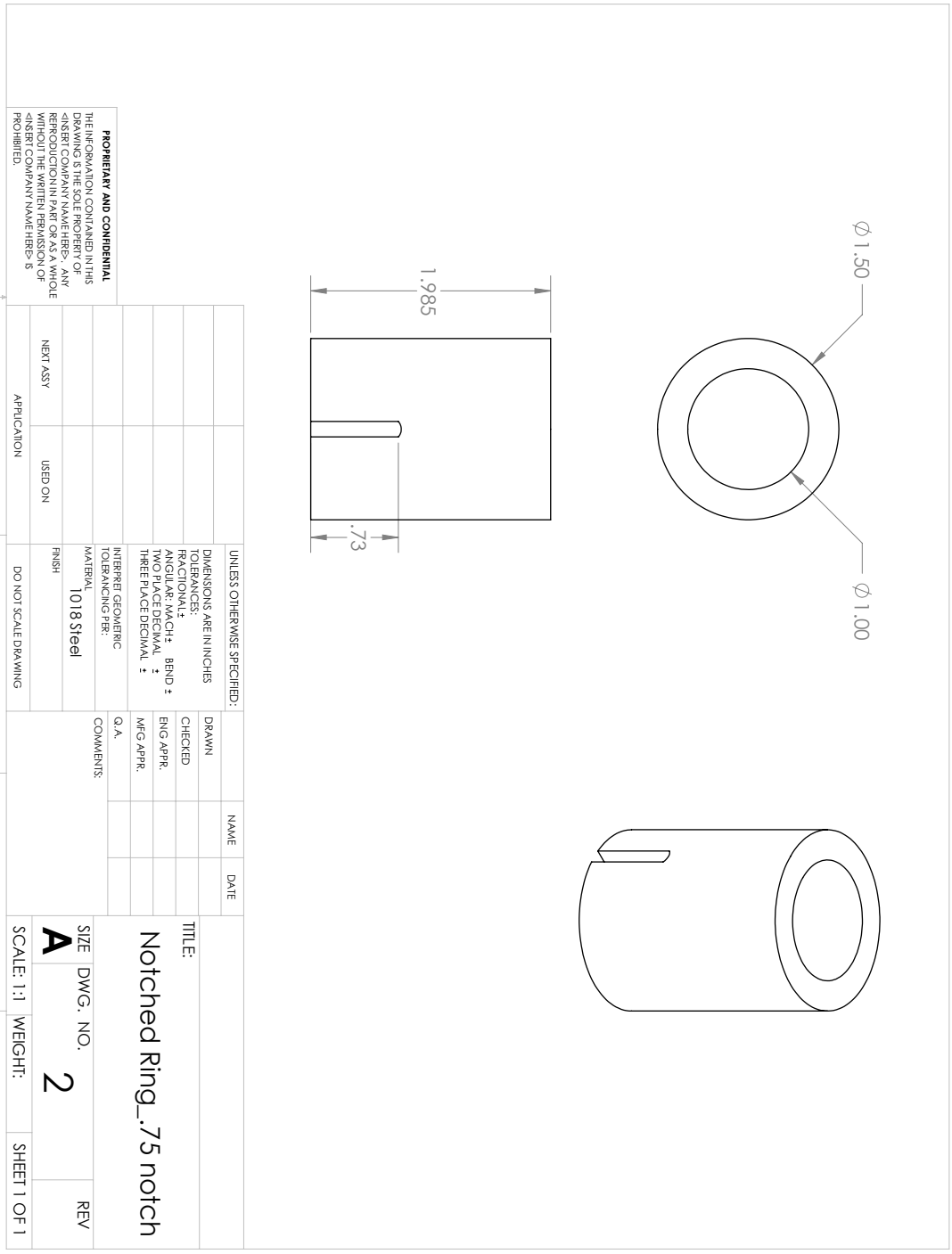

Figure 0.12: MFI Tall Ring

Figure 0.13: MFI Tall Rod

ITEM NO.	PART NAME	DESCRIPTION	QTY.
1	Rod	1018 Steel	1
2	Notched Ring_.75 notch	1018 Steel	1
3	Terfenol	$Tb_3Dy_7Fe_2$	1
4	Spool	Aluminum	1
5	Coil	Magnet Wire: size 26 AWG, 300 turns	1
6	Base	1018 Steel	1

UNLESS OTHERWISE SPECIFIED:
DIMENSIONS ARE IN INCHES
TOLERANCES:
FRACTIONAL ±
ANGULAR: MACH ± BEND ±
TWO PLACE DECIMAL ±
THREE PLACE DECIMAL ±
INTERPRET GEOMETRIC TOLERANCING PER:
MATERIAL
FINISH
DO NOT SCALE DRAWING

	NAME	DATE
DRAWN		
CHECKED		
ENG APPR.		
MFG APPR.		
Q.A.		
COMMENTS:		

APPLICATION
USED ON
NEXT ASSY

TITLE:
Magnetic Field Insulating Fixture
Tall Assembly w .75" spool

SIZE A | DWG. NO. | REV
SCALE: 1:1 | WEIGHT: | SHEET 1 OF 1

Figure 0.14: MFI Tall Assembly

APPENDIX B

GUI AND MTS SOFTWARE SETUP

0.1 Graphical User Interface Design

An example of the GUIDE used to create this particular GUI can be seen in Figure 0.15.

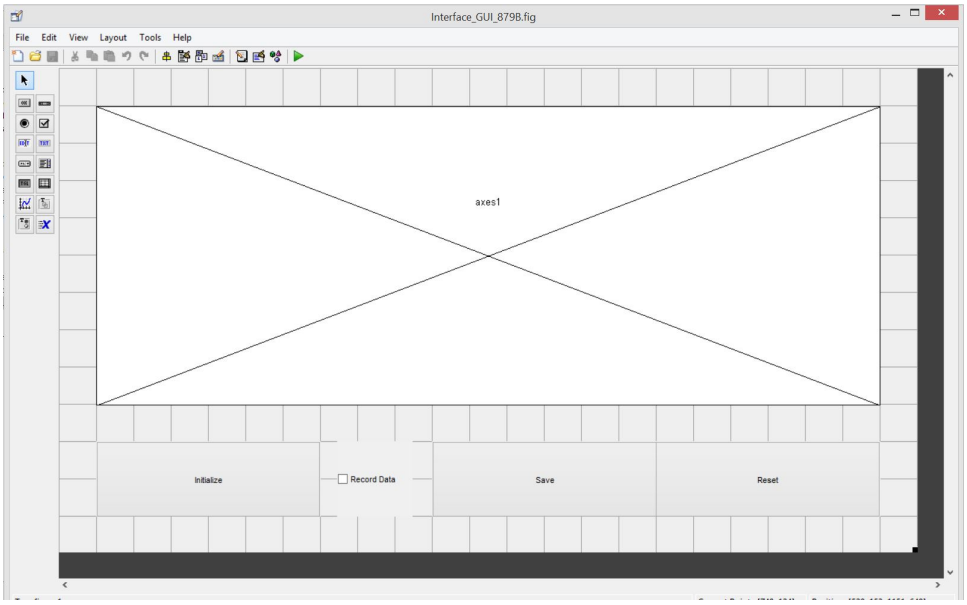

Figure 0.15: GUIDE

The GUI built needs to be simple enough for anyone to operate, yet intuitive as to prevent loss of data or improper initialization. To properly establish connection with the meter the built in MATLAB function instrfind is used with the configuration indicating a serial communication on USB port name COM3. After which it is necessary to set the meter to measure inductance with the appropriate frequency. This is achieved through a few simple commands shown:

```
obj1 = instrfind('Type', 'serial', 'Port', 'COM3', 'Tag', '');
query(obj1, 'FUNCtion:impa L');
query(obj1, 'FREQuency 10000');
```

Once the connection is established, the rest of the parameters necessary for data transmission are automatically retrieved by the MATLAB function:

Serial Port Object : Serial-COM3

Communication Settings

Port: COM3

BaudRate: 9600

Terminator: 'LF'

Communication State

Status: closed

RecordStatus: off

Read/Write State

TransferStatus: idle

BytesAvailable: 0

ValuesReceived: 319

ValuesSent: 109

A real-time plot of the inductance vs time is necessary to confirm the sensor is working correctly. This is done by updating the plot every time a measurement is taken. The buttons were kept to a minimum to maximize simplicity with different states indicated by distinct colors. Once the program is initialized, the button becomes red to signify that the meter is being communicated with, seen in Figure 0.16. Once finished establishing a connection with the meter, the button becomes green indicating it is ready to begin recording, as shown in Figure 0.17.

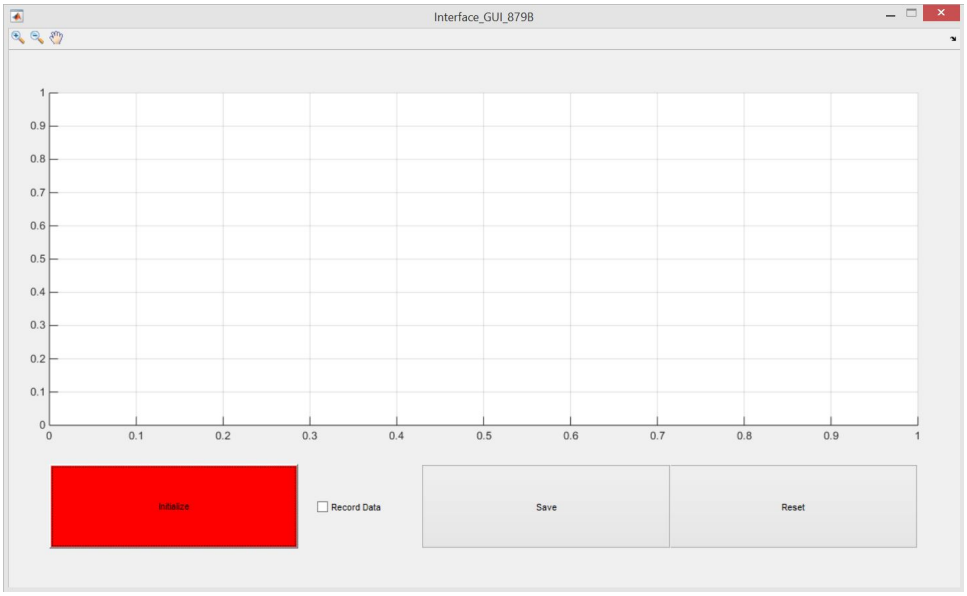

Figure 0.16: GUI Initializing

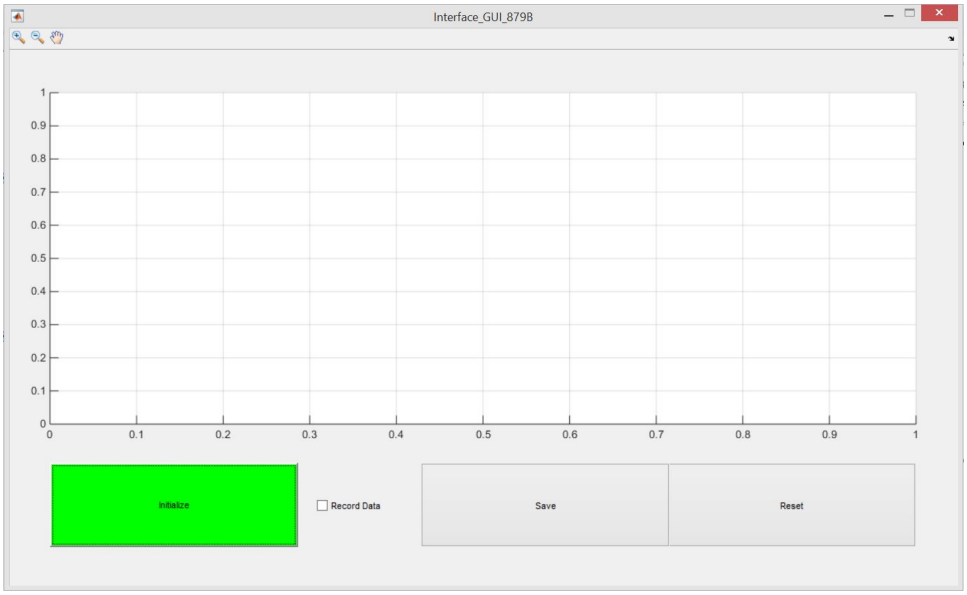

Figure 0.17: GUI Initialized

Once fully initialized, the GUI will be able to interact with and take readings from the meter. This is achieved by selecting record data on the GUI. Once the checkbox is selected, the time of the computer will be recorded and the meter will begin recording inductance and taking the respective time of each reading. This is done through the use of a query function that fetches the current value

being recorded on the meter:

```
data1 = query(obj1,'FETCh?');
```

To ensure that the operator does not try to save the data or reset the GUI until the recording has stopped, several precautions are taken. Not only do the buttons become red deterring theoperator from pressing them, but a warning also pops up if the data is not saved before resetting the meter. These instances are shown in Figure 0.18 and Figure 0.19.

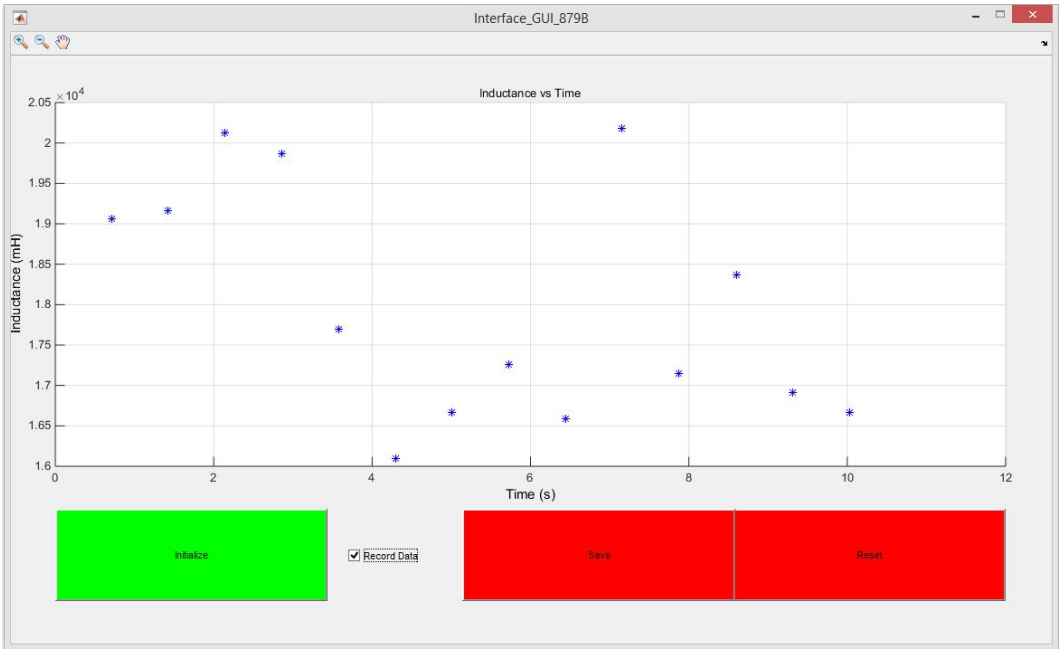

Figure 0.18: GUI Recording

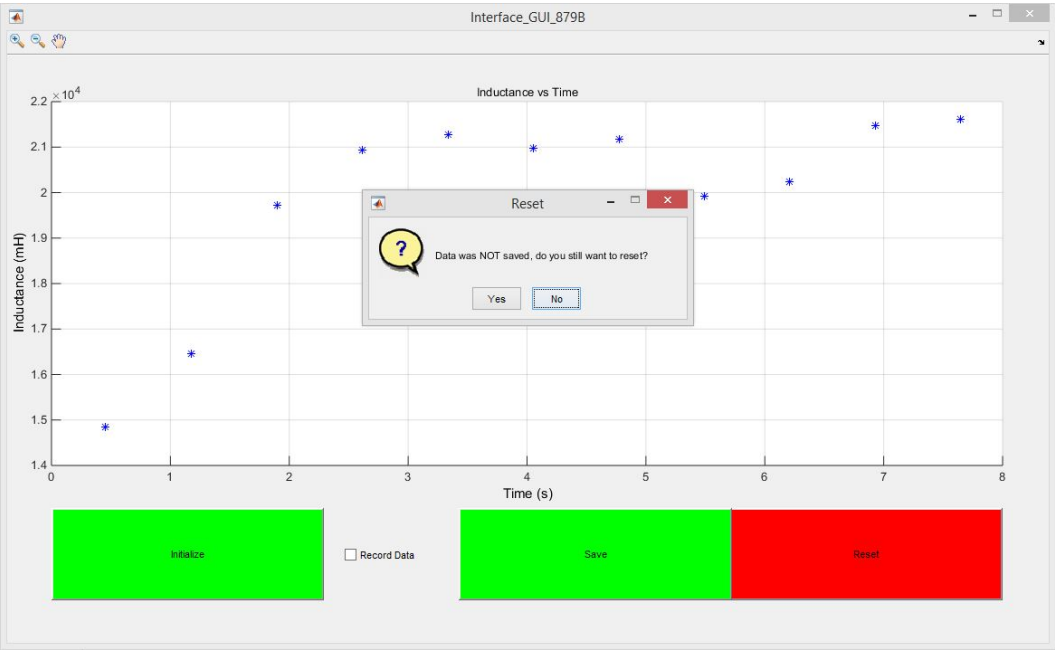

Figure 0.19: GUI Warning

0.2 Material Test System

The configuration for the material test system is shown in Figure 0.22.

Figure 0.20: MTS

Figure 0.21: MTS Controller

Figure 0.22: Flex Test 40 setup

The initial experiments for calibration and material characterization were carried out using the manual control, after which, more control was deemed necessary for future experiments. The Flex

Test 40 Controller is interfaced with through two different programs: Multi-Purpose Testware and Test Works 4. Testworks 4 is initially chosen for its simple interface and built in procedures. A sinusoidal load cycle is used with limits set in pounds and a rate set in inches per minute. The interface as well as the parameter setting is shown in **??** and Figure 0.24 respectively.

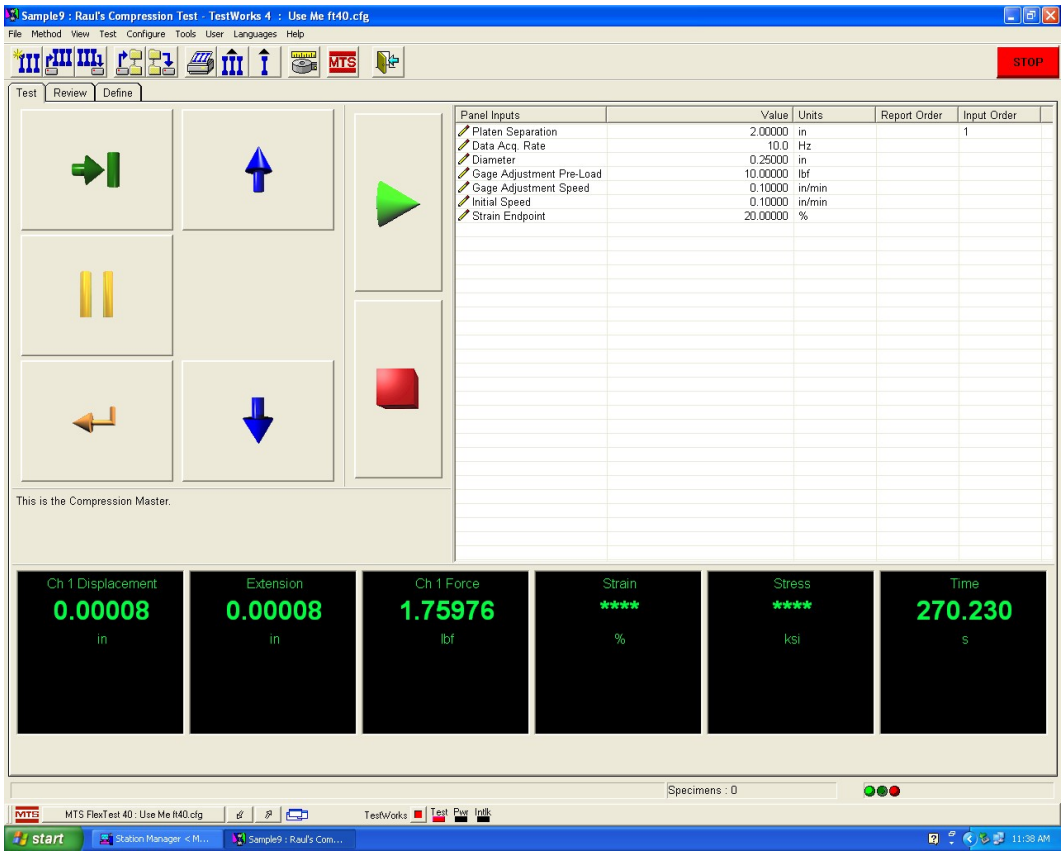

Figure 0.23: Test Works 4 Interface

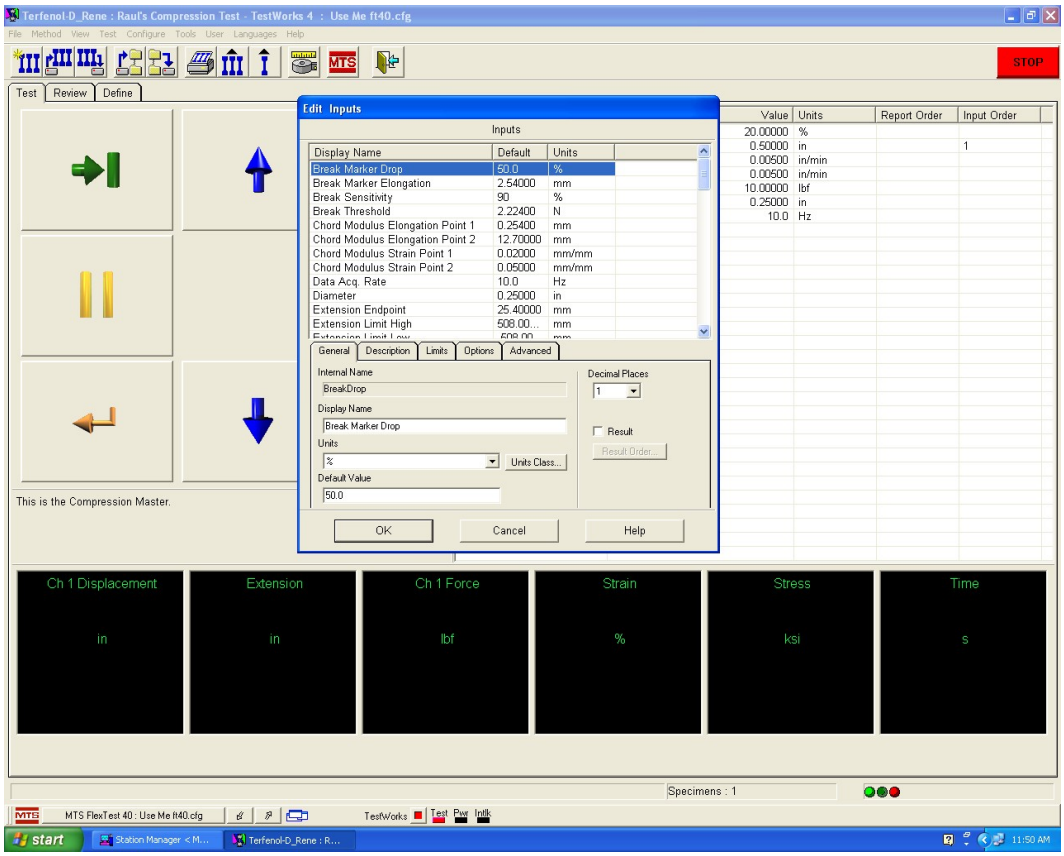

Figure 0.24: Test Works 4 Parameter Setting

Unfortunately, the level of control given by the limited license of Testworks available was not sufficient for the experiments necessary for proper calibration of the sensor being developed. When speed is raised beyond a certain point, the load begins to overshoot the limits causing predictable damage to the rods. It is for these reasons that the switch to the Multi-Purpose Testware was made. With this software a greater control of the parameters and function of the MTS is attained. An example of the configuration of the software is shown in Figure 0.25. The procedures are built using a variety of pre-designed templates, giving you the ability to control limits and speeds using displacement, load, and acceleration in both metric and imperial units of measurement. A example of a procedure set up can be seen in Figure 0.26.

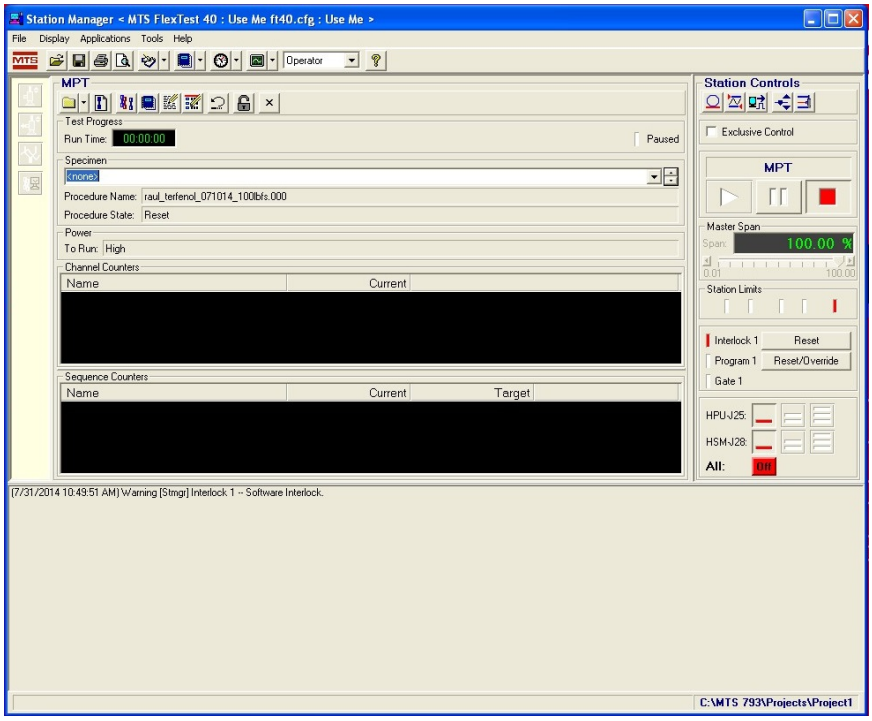

Figure 0.25: Multi-Purpose Testware Interface

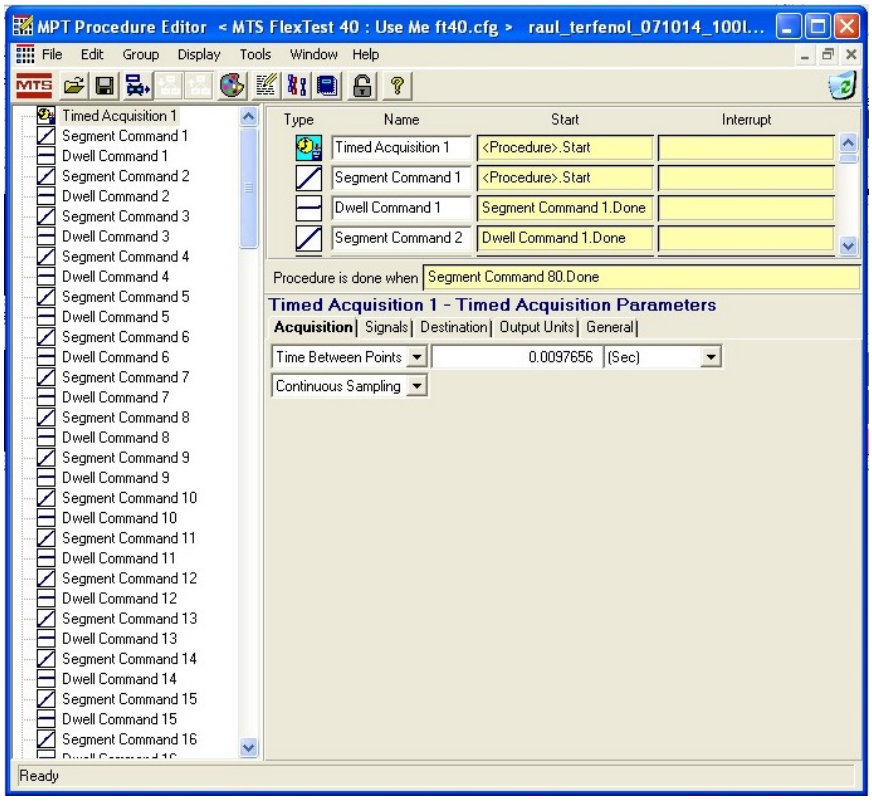

Figure 0.26: Multi-Purpose Testware Procedure

BIOGRAPHICAL SKETCH

Raul Estrada was born on November 11, 1990 in El Paso, TX to Mr. Javier Estrada and Mrs. Maria Del Carmen Estrada. He graduated from the Science Academy of South Texas in 2004. Since then, he has attended the University of Texas Pan American where he earned his Bachelor's degree in Electrical Engineering in Spring of 2012. He went on to further his education and pursue a Master's of Science degree in Electrical Engineering, which is to be completed in Fall of 2014. While at UTPA, he held a number of positions from Call Center supervisor to research assistant to teaching assistant. Raul Estrada can be reached at raul.g.estrada@gmail.com or 500 W. Hibiscus Ave., Mcallen, TX, 78501.